Journal of Energy Storage 56 (2022) 106000

Contents lists available at ScienceDirect

Journal of Energy Storage

journal homepage: www.elsevier.com/locate/est

Research Papers

Recent advances in aqueous redox flow battery research

Ayodeji Adeniran [a], Alex Bates [b], Nicholas Schuppert [a], Ashwin Menon [c], Sam Park [a,*]

[a] Department of Mechanical Engineering, University of Louisville, United States of America
[b] Energy Storage Research Group, Sandia National Laboratories, United States of America
[c] Department of Mechanical Engineering, Case Western Reserve University, United States of America

ARTICLE INFO

Keywords:
Redox flow battery
Aqueous
Recent advances
Electrolyte
Membrane
Electrode

ABSTRACT

The aqueous redox flow battery (RFB) is a promising technology for grid energy storage, offering high energy efficiency, long life cycle, easy scalability, and the potential for extreme low cost. By correcting discrepancies in supply and demand, and solving the issue of intermittency, utilizing RFBs in grid energy storage can result in a levelized cost of energy for renewable energy sources that is competitive with non-renewable energy sources. With RFBs, the hope for the proliferation of renewable energy sources continues. In this review, recent advances in aqueous RFBs are explored, highlighting novel chemistries, configurations, and the current standard in operating current density and energy efficiency. This review contrasts the advantages and disadvantages of various aqueous RFB systems, while bringing attention to major challenges facing the technology. In addition, the current research trend and direction of RFBs are made apparent.

1. Introduction

Due to the intermittent nature of renewable energy sources, an energy storage device is necessary to level the imbalance in supply and demand. With a low-cost, high efficiency, and long cycle life energy storage device, renewable energy use in grid energy applications will proliferate. Of the possible grid energy storage technologies, redox flow batteries (RFB) have been widely recognized as being uniquely fit for the job. The RFB is a type of electrochemical cell used to convert chemical energy into electrical energy by flowing an electrolyte solution across the surface of an electrode. At the electrode surface, a redox species is oxidized or reduced. RFBs are separated by an ion-exchange membrane into two half-cells. The ion-exchange membrane allows specific ions to freely cross, balancing the cells charge, while preventing the active species from crossing. In the half-cell containing the anode, the electrolyte solution is termed the anolyte. Similarly, in the half-cell containing the cathode, the electrolyte solution is termed the catholyte. Through this process of electrolyte flow, oxidation and reduction, and ion-exchange, electrons are driven through an external circuit, bringing electricity in, to be stored, or releasing it. A schematic of a general RFB is shown in Fig. 1(a). The schematic highlights the external electrolyte storage tanks and electrochemical cell. As seen in Fig. 1(a), redox species A is reduced during charge and redox species B is oxidized during charge.

RFBs are typically utilized as a secondary battery but, they can act like a fuel cell, where new fuel is continually provided for conversion to electricity. RFB technology has been marketed for use in grid energy storage. The key difference between RFBs and other secondary batteries is the ability to store the electrolyte solution externally, separated from the electrochemical cell. This unique feature allows for the separation of energy and power so the either can be scaled independently. In this way, the energy storage capacity can be increased by simply adding additional electrolyte fluid. RFBs can be easily scaled to meet specific energy storage needs. This feature provides RFBs a distinct advantage in grid energy storage of intermittent energy sources.

A French patent by Pierre André Pissoort, published in 1933, is the first recorded notion resembling the modern day RFB [5]. The next mention of the RFB, which describes the concept explicitly as it is thought of today, comes from a German patent by Walther Kangro published in 1954 [6]. Following this was a publication in 1955 by Posner titled “Redox Fuel Cell”. A hybrid zinc-air flow battery with a flowing liquid electrolyte was tested in 1966 by Vertes et al. [7,8]. In the 1970s, RFB research really began to take off with research by the National Aeronautics and Space Administration (NASA) in the USA, as well as groups in Japan and France [9–15]. In the 1980s, the now commercialized all-vanadium RFB by Maria Skyllas-Kazacos made its debut [16]. Today, the number of publications exploring different aspects of RFBs is ever increasing. The focus of current research is on a wide

* Corresponding author.
E-mail address: sam.park@louisville.edu (S. Park).

https://doi.org/10.1016/j.est.2022.106000
Received 27 May 2022; Received in revised form 7 October 2022; Accepted 26 October 2022
Available online 2 November 2022

variety of redox couples, configurations, material improvements, and optimizations; however, the most highly researched RFB remains the all-vanadium, aqueous RFB.

The fastest growing energy source in the world is renewables, with an average increase in consumption of 2.3 % year^{-1}; however, non-renewable sources are still projected to account for 77 % of energy use in 2040 [17]. This statistic makes it apparent that the renewable energy industry still has a long way to go before overtaking non-renewables in the grid energy market. A major problem with renewable energy sources such as wind and solar, two of the most promising renewables, is their intermittent nature. If energy is not consumed when the wind blows and the sun shines, it must either be stored or wasted. To make wind and solar cost competitive with non-renewables, not only must the renewable energy source become more efficient, the storage of excess energy must also become more efficient. In addition, without a grid energy storage solution, renewable sources will always be dependent on non-renewables to compensate when the driving force of the renewable (e.g. wind) is not present. A highly efficient and long cycle life grid energy storage solution is essential for renewable energy sources if the goal is 100 % renewable energy. In terms of a RFB, power density requirements determine the size of the electrochemical cell and energy density determines the size of the electrolyte storage.

In 2016 pumped hydro energy storage (PHES) accounted for over 95 % of global energy storage due to its maturity, cost, and efficiency [18]. New capabilities allow PHES systems to operate within a max efficiency of 76–85 % [19]. A PHES is a matured technology and a considerable efficiency margin is presented. However, it requires the specialist nature of the site required, needing both geographical height and water availability. Additionally, PHES systems suffer from location dependence. A proposed location must have suitable geography that allows for an elevated reservoir, without damaging the surrounding natural habitat; otherwise PHES becomes cost prohibitive. This significantly limits the ability of PHES technology to be implemented as a solution to grid energy storage worldwide. Fig. 2(b) shows a comparison of efficiency values for currently competitive grid energy storage solutions. On the scale of grid energy storage, efficiency is paramount. Each percentage point of efficiency can relate to 1000 s of kWh, depending on the size of the system. Worldwide, that number becomes astronomical. Redox flow batteries compare well with other grid energy storage technologies, especially those considered long-term. RFB technology is in its infancy, with vast room for improvement in terms of technological advancements and optimization.

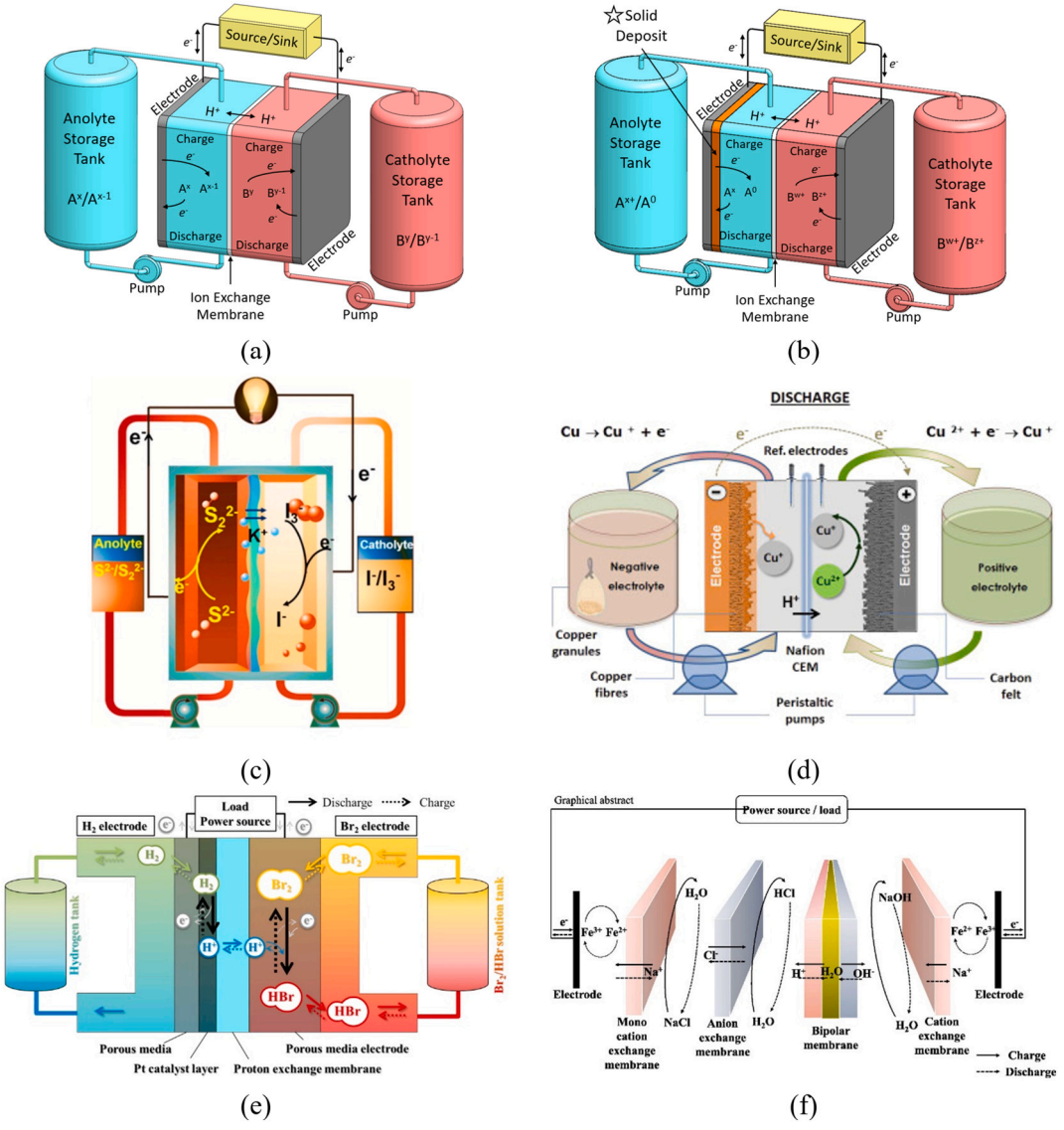

Fig. 1. Schematic of (a) an all-liquid redox flow battery, (b) a hybrid RFB highlighting the solid deposition phase, (c) a high energy density iodine-sulfur RFB, (d) an all-copper RFB, (e) a hydrogen-bromine RFB, and (f) an acid-base junction flow battery [1–4].

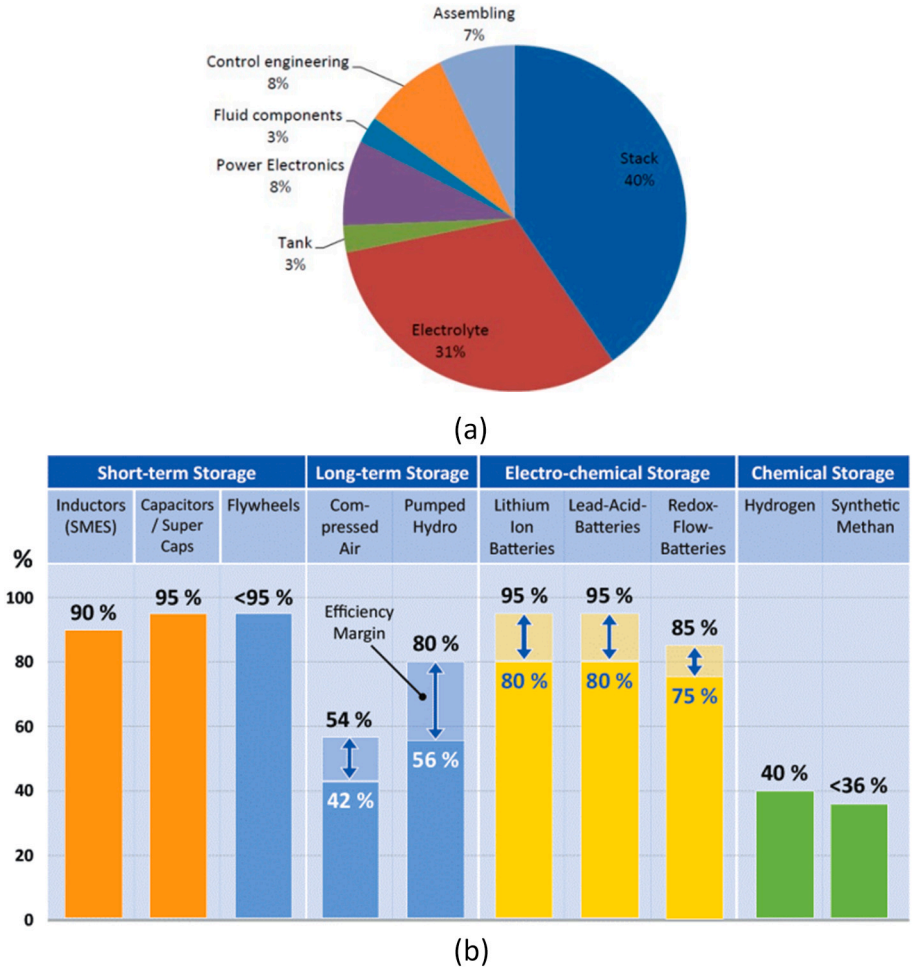

Fig. 2. Redox flow battery performance and cost metrics including (a) cost separation of the different components making up an all-vanadium RFB, and (b) expected energy efficiency of competitive grid energy storage solutions [20,21].

RFBs offer the promise of surpassing PHES in terms of cost and efficiency, which stands to catapult the profitability of renewable energy sources well beyond non-renewable sources. RFBs with energy efficiencies above 90 % have already been reported in literature [22,23]. Additionally, RFBs do not have a geographical dependence. In fact, they are quite flexible in orientation, even compared to other secondary batteries like Li-ion. They are also safe in comparison to Li-ion and do not require the safety features and climate control necessary for an array of Li-ion batteries. In the past, concerns for RFBs have been over cost of the active species and/or the ion-exchange membrane required in the electrochemical cells, as well as the safety of the corrosive electrolyte. Increasingly, safe and cost-effective chemistries are being explored [3,24–28]. Fig. 2(a) shows the cost separation of a standard all-vanadium RFB. The share of the cost in a RFB is strongly affected by its energy to power ratio [29]. The largest cost component of the electrolyte is due to the active species, and for the stack, or electrochemical cell, it is the ion-exchange membrane. Driving down these costs, through either technological advancement or replacement with cost-effective alternatives, can significantly drive down the already competitive levelized cost of energy for RFBs.

As RFB research has exploded in recent years, it has become difficult to keep up with current research efforts and their redox couples and battery configurations. Non-aqueous RFB research is beginning to rival aqueous research in terms of research volume, due to the plethora of solvents and redox couples that can be explored. In the non-aqueous organic category of RFB research, nearly infinite combinations exist and with them, the need to filter and explore the worthwhile from the worthless. Non-aqueous RFBs, compared to aqueous RFBs, have a low coulombic efficiency, low ionic conductivity, and low solubility of active species [30–32]. Non-aqueous RFBs often employ flammable and expensive organic solvents [30–32]. The notion that aqueous RFBs are still the future from a cost and safety perspective, leads to the focus on recent developments in aqueous RFB research [30–32].

The purpose of this review paper is to summarize recent research work in RFBs, focusing on aqueous electrolytes including the all-vanadium, iron-vanadium, iron-chromium, iodine-sulfur, cobalt-tungsten, manganese, and ferri/ferrocyanide all-liquid RFBs. Demonstrated hybrid RFBs include all-copper, copper-iron, iron-cadmium, lead-iron, cerium-lead, all-lead, iron-zinc, iodine-zinc, zinc-bromine, zinc-cerium, cadmium-organic, sulfur-air, and hydrogen bromine. Specialized RFBs include the semi-solid all-iron, organic all-sodium, organic zinc-TEMPOL, organic cyclohexanedione, membrane-less zinc-quinone, concentration gradient, acid-base junction, and solid charge storage.

In keeping with the rise in RFB research, many other reviews have been published on the topic. Two notable reviews, published by Leung et al. and Wang et al., respectively, provided a comprehensive analysis of the state of RFB technology in the years 2012 and 2013 [33,34]. However, this review incorporates research conducted in the years since, including articles from the past three years. More recent reviews provide a more accurate assessment of current technology, although certain aspects lack detail. The 2017 article by Li et al. failed to provide a comprehensive review of specific redox couples; the 2020 article by Gentil et al. focused on aqueous organic RFB (AO-RFB), the 2020 article by Zhang et al. also focused on iron based aqueous RFB, while this paper

includes a holistic research into both organic and inorganic redox couples [24,25,35,36].

2. Redox flow battery categories

As RFB technology has advanced and grown, categorizing different types of RFBs became necessary. RFBs are typically categorized based on some key aspect of their operation, such as the phase of the electrolyte or the types of molecules employed; instead of focusing on the specific redox couples that are used. However, not all configurations fit neatly into a category, and some straddle multiple categories as they are defined in this review. When considering the electrolyte phase, there are two main categories separating RFB configurations: the all-liquid and the hybrid RFB. These categories are defining because, in general, they split RFBs based on one of its most important characteristics, the separation of power and energy. For a hybrid RFB, increasing the energy storage capacity is not as simple as increasing the volume of electrolyte.

In an all-liquid RFB, which includes the well-known all-vanadium RFB developed by Skyllas-Kazacos, both anolyte and catholyte remain in the liquid phase during charge and discharge [16]. For the vanadium example, vanadium ions transfer between the V^{2+} and V^{3+} oxidation states in the anolyte and the V^{4+} and V^{5+} oxidation states in the catholyte; the ions remain in solution during the process. Some all-liquid RFBs employ a single chemical, such as vanadium, as both the anolyte and catholyte active species. Crossover is an event that results in capacity loss for a RFB so, it is important that it is avoided. Crossover can also result in the mixing of active species that is difficult to recover and, sometimes, irreversible side reactions. When one chemical species is employed in both half-cells, termed a mixed electrolyte, crossover due to diffusion is reduced. Diffusion is ion movement resulting from a concentration gradient. In a mixed electrolyte, both anolyte and catholyte active species are mixed into a single electrolyte that is employed in each half cell. The anolyte active species is not active in the catholyte and vice versa. The use of a mixed electrolyte is becoming the standard in reducing crossover when different chemical species are utilized in each half-cell. In the case of the all-vanadium RFB, the anolyte and catholyte can simply be remixed to rebalance the electrolytes. This certainly results in a loss of stored energy but, it is relatively simple to implement and is a far better alternative to irreversible side reactions.

The hybrid RFB category, shown in Fig. 1(b) in the introduction, utilizes a non-liquid phase active species. Fig. 1(b) emphasizes a solid deposit on the anode electrode. It is typical but, not required, for the solid phase deposition to occur on the anode during charge in a hybrid RFB. As the solid deposits on the electrode, it becomes the electrode itself. This can be an advantage or disadvantage depending on the deposits overpotential to hydrogen evolution and resistance to corrosion. The hybrid RFB category can be further separated into RFBs with a gas phase active species and RFBs in which a plating reaction occurs; however, RFB consisting of at least one gas phase are relatively rare.

A well-researched example of a hybrid RFB is the zinc-bromine RFB. The anolyte solution containing Zn^{2+} ions in its discharged state undergoes electrodeposition at the anode to become solid zinc, Zn^0. At the cathode, bromine remains as a solution. Due to the solid phase deposition, the charged, active species can no longer flow out of the electrochemical cell, recoupling power and energy. The amount of energy stored is dependent on the accessible plating volume, which is dependent on electrode and ion-exchange membrane spacing. Additional plating volume can be obtained by increasing the gap between electrode and ion-exchange membrane; however, this comes with an efficiency cost due to ion transport and electrolyte conductivity. Another major disadvantage inherent with most plating reactions is dendrite formation. Dendrites are tentacle-like growths in the deposited layer that tend to grow and extend through the gap between the electrode and ion-exchange membrane as cycling occurs. If the dendrite pierces the ion-exchange membrane, mixing of the active species in each half-cell will occur. A short-circuit of the cell results when the dendrite reaches the cathode, resulting in complete failure of the RFB.

The previously described categories are based on the electrolyte phase. Other ways of categorizing RFBs include separation based on the class of electrolyte solvent or active species. For instance, RFBs can be separated by those with an aqueous electrolyte solution and those with a non-aqueous electrolyte solution. Based on the active species, RFBs can be separated into non-organic and organic. These categories became necessary recently due to an increase in research of organic redox couples and non-aqueous solvents. Organic, tunable, active species have gained interest recently as their characteristics can be adjusted based on the needs of the system. Unfortunately, these molecules tend to be large and complex. The molecule size can result in low solubility and/or high viscosity, both undesirable for RFBs. The complexity of an organic molecule tends to result in multiple reaction pathways and expensive synthesis techniques. In addition, organic molecules usually require non-aqueous solvents. Non-aqueous solvents are generally expensive compared to water and hazardous (e.g. flammable).

Beyond these categories are some unique RFB configurations including the membrane-less and solid charge storage RFB. Two other types of flow batteries that are being explored are the concentration gradient and acid-base junction batteries. Each category has its own unique set of advantages and disadvantages. Membraneless RFBs were developed to remove the expensive ion-exchange membrane from the cell. The technology reviews herein will be organized by chapter as follows; Chapter 3 includes the all-liquid RFBs without any organic redox species, Chapter 4 includes the hybrid RFBs without organic redox species, Chapter 5 includes any RFBs which contain an organic species, and Chapter 6 includes any specialized flow battery technologies that do not fit into the previous chapters. Chapter 7 will then summarize current research trends and technical issues within aqueous electrolyte RFB research.

3. All-liquid redox flow batteries

3.1. All-vanadium

The all-vanadium RFB was developed in 1986 by Skyllas-Kazacos et al. and since then has been commercialized and researched more than any other chemistry or configuration [16]. The anolyte and catholyte in the all-vanadium RFB both contain vanadium as the active species; V^{2+}/V^{3+} in the anolyte and V^{4+}/V^{5+} in the catholyte. The supporting electrolyte is typically sulfuric acid in high concentration which provides stability to the active species and good ionic conductivity. Skyllas-Kazacos et al. developed the all-vanadium RFB using a 2 mol/L H_2SO_4 which had a discharge current density of 3 mA/cm^2 [16]. With the all-vanadium RFB, crossover of vanadium ions across the ion-exchange membrane does not cause irreversible side reactions, as in many other RFB chemistries. Crossover does lead to a loss in coulombic efficiency and capacity; however, the balance of ions in the half-cells is easily recoverable by mixing. The energy density of the all-vanadium RFB is based on the solubility of each vanadium ion species. The solubility limit of vanadium is also dependent on the concentration of the supporting electrolyte; an increase in sulfuric acid concentration increases conductivity; but, decreases vanadium solubility. The all-vanadium RFB has a limited operating range due to precipitation of V_2O_5 at higher temperatures. The all-vanadium RFB also suffers from efficiency losses due to gas evolution, specifically hydrogen evolution at the anode.

$$VO_2^+ + 2H^+ + e^- \leftrightarrow VO^{2+} + H_2O \qquad 0.991 \text{ V vs.SHE} \tag{1}$$

$$V^{3+} + e^- \leftrightarrow V^{2+} \qquad -0.255 \text{ V vs.SHE} \tag{2}$$

The following subsections have been included to separate the vast amount of all-vanadium research that has recently been conducted.

3.1.1. Electrochemical cell design

In recent years, research has focused on improving the limitations of the all-vanadium RFB through enhanced electrodes, new ion-exchange membranes, and improved cell designs. Zheng et al. developed a novel circular vanadium flow battery (CFB), Fig. 3(a), to improve on mass transport limitations by reducing concentration polarization, which exists in conventional rectangular flow batteries and, as a result, increasing electrolyte utilization [37]. At high current densities, concentration polarization is more pronounced. This issue has been tackled in the past by increasing the electrolyte flow rate; however, that comes at the cost of increased pump consumption. Using a circular design, with the inlet along the outer radial surface and outlet along the inner radial surface, offers a shorter path length and increased velocity near the outlet which improves mass transport, without increasing pump consumption [37]. The CFB shows an increased electrolyte utilization of 10.52 % at 40 mA cm^{-2} and 30.46 % at 160 mA cm^{-2} [4]. Ressel et al. developed a vanadium flow battery with a tubular cell design to reduce manufacturing costs and shunt current losses [38]. The tubular cell design offers decreased sealing path length compared to conventional flow battery designs; however, during experiments, it suffered from high ohmic overpotential [38].

Some researchers have sought to focus on the design of the flow path as opposed to the cell architecture. Houser et al. performed a design optimization study on the all-vanadium RFB to examine the effects of flow field design [42]. They found that there is no one optimal path but, that it is dependent on the operating conditions, electrode, and electrolyte properties. At low flow rates the interdigitated design was best and as the electrode thickness increased, the serpentine design improved compared to the interdigitated design [42]. Reed et al. examined ways to optimize a kW class all-vanadium RFB by changing the membrane, switching from a flow-through (without a flow field) design to flow-by (interdigitated), and controlling the electrolyte temperature [43]. They found that a woven carbon fiber cloth with a non-porous flow frame offered performance enhancements. With the new design they obtained an energy efficiency of 74.2 % at 320 mA/cm^2 [43]. Kumar et al. tested the all-vanadium RFB with three different flow fields (flow through, serpentine, and interdigitated) while holding all other operating conditions constant [44]. They found that the serpentine flow field performed the best with the lowest pressure drop and an energy efficiency of 80 % [44]. Bhattarai et al. explored the use of cutting flow channels into the porous electrode, shown in Fig. 3(b), to improve flow distribution while maintaining or reducing pump power requirements [40]. They found that interdigitated channels cut directly into the graphite felt can improve overall energy efficiency up to 2.7 % [40].

A more significant deviation in cell design, the inclusion of photocharging, was explored by several groups. Photocharging attempts to use a photoelectrochemical process to change the oxidation state of an active species directly. This process attempts to skip the middleman, so to speak. That is, it skips the process of producing electricity in photovoltaic cells, and then storing that electricity in an electrochemical cell.

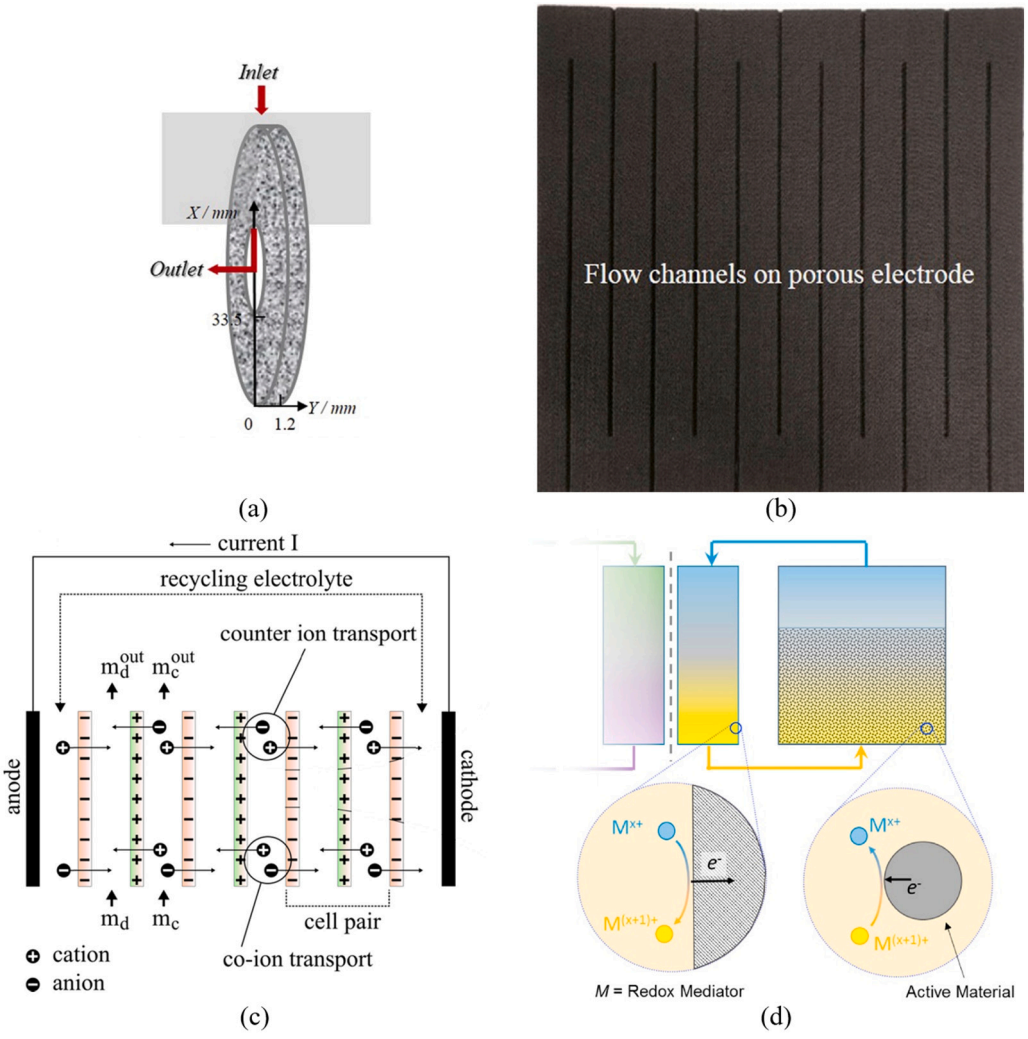

Fig. 3. Novel and unique designs including (a) a circular RFB design with the electrolyte inlet on the outer radius and outlet on the inner radius, (b) flow channels cut directly into a porous graphite electrode, (c) a concentration gradient flow battery, and (d) a solid charge storage flow battery [37,39–41].

Liao et al. explored the use of charging the vanadium redox couples using photoelectrochemical regeneration where a TiO_2 photoelectrode is placed directly in the catholyte [45]. The photocharging occurred at a potential of 0.1 V and discharge of the redox couple occurred at 23.0 mWh L^{-1} with 67.4 % of that as recovered solar energy [45]. Wei et al. tested the use of ultra-long TiO_2 nanobelts on a vanadium photoelectrochemical storage cell [46]. The photon-to-current efficiency was ~22 % without any external bias [46]. Shen et al. explored the use of dye sensitized TiO_2 nanobelts in a vanadium photoelectrochemical storage cell [47].

3.1.2. Electrode modification

To increase overall energy efficiency, by reducing activation overpotential through improved electrocatalytic activity and/or reducing gas evolution, researchers have examined enhancing the electrode. Kabtamu et al. experimented with a water activation method to enhance the electrochemical activity of graphite felt for use in an all-vanadium RFB [48]. They prepared the graphite felt using water vapor injection at 700 °C for 5 min [48]. The process produced high contents of oxygen-containing functional groups on the graphite fibers, which are known to be electrochemically active towards vanadium. They achieved an energy efficiency of 83.10 % at 50 mA cm^{-2} with the treated graphite felt electrodes [48]. González et al. developed a graphene-modified graphite felt, shown in Fig. 4(a), from raw graphite felt and a graphene oxide water suspension using electrophoretic deposition [22]. This modified graphite felt enabled the group to obtain an energy efficiency of 95.8 % at 25 mA cm^{-2} in an all-vanadium RFB [22]. The graphite felt modified with graphene exhibited a 3D cross-linked structure with increased wettability and active area for the vanadium redox reaction. In addition, the graphite felt fibers connected with graphene, improving charge transfer. Chen et al. used atmospheric pressure plasma jets to modify a graphite electrode for use in an all-vanadium RFB [49]. The plasma improves wettability throughout the graphite felt, increasing electrolyte contact. It was found that the plasma treatment improved the oxygen-containing groups and introduced nitrogen into the graphite felt, which enhances electrochemical

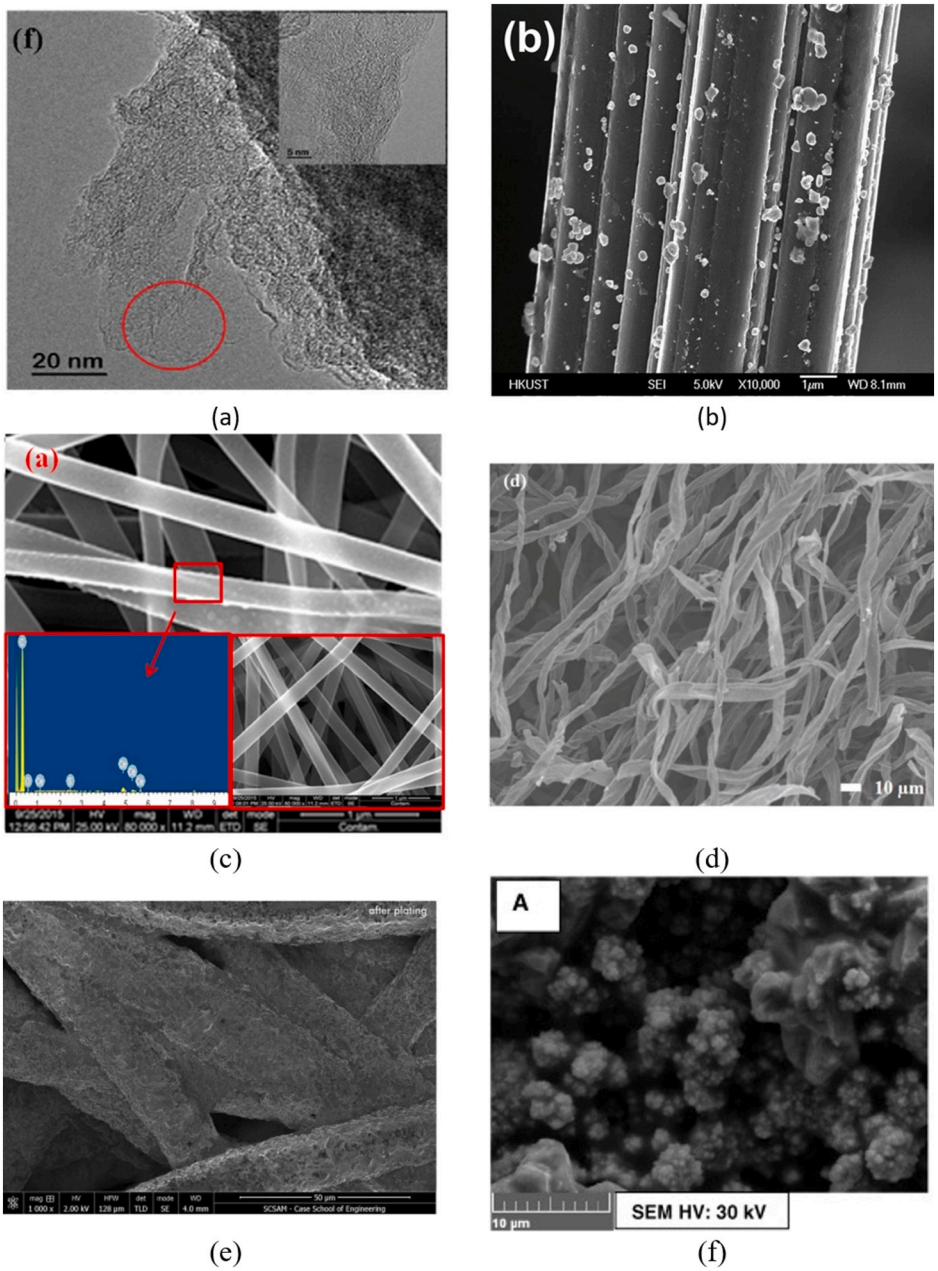

Fig. 4. Electron microscopy images of modified electrode materials including (a) graphene-modified graphite felt resulting in an extremely high energy efficiency all-vanadium RFB, (b) copper nanoparticle coated graphite felt fiber resulting in a high operating current density while maintaining a reasonable energy efficiency, (c) electrospun carbon nanofibers with CeO_2 nano particles on their surfaces, (d) biomass derived, carbonized cotton electrode, (e) copper plating of carbon fibers in a copper-iron RFB, and (f) cadmium deposition on a copper electrode [22,50,57,59–61].

reactivity. Chen et al. achieved an energy efficiency of 76 % at 80 mA cm^{-2} [49].

Wei et al. developed a copper nanoparticle coated graphite felt electrode, Fig. 4(b), for testing in an all-vanadium RFB [50]. The all-vanadium RFB achieved an energy efficiency of 80.1 % at a current density of 300 mA cm^{-2}; a result of increased voltage efficiency due to the copper plating of the graphite felt [50]. The copper nanoparticles are electroplated and dissolved during each charge/discharge cycle, respectively. Kim et al. examined the effects of adding a tungsten catalyst to the electrolyte that is subsequently electrodeposited onto the electrode [51]. The group found that the addition of tungsten improved the energy efficiency of the all-vanadium RFB by 3 %, resulting in an energy efficiency of about 85 % at 40 mA cm^{-2} [51]. Wei et al. developed a titanium nitride nanowire coating on a graphite felt electrode for testing with an all-vanadium RFB as the anode [52]. The nanowires are grown onto the surface of the graphite felt by a seed-assisted hydrothermal process and converted to titanium nitride through a nitridation reaction. The modified electrode, all-vanadium RFB achieved an energy efficiency of 77.4 % by increasing the vanadium reaction kinetics and creating larger active sites for reaction [52]. Wei et al. obtained an energy efficiency of 84.8 % at 100 mA cm^{-2} using a carbon nanoparticle-decorated graphite felt electrode and a serpentine flow-field structure [53]. The flow-by structure reduces ohmic losses by reducing the electrode thickness. The carbon nanoparticle coating increased surface area and improved electrocatalytic activity.

Kabir et al. studied the effects of oxidizing pyrolytic graphite for 1 min in 1 M H_2SO_4, used as the anode [54]. This process increases the number of oxygen containing functional groups on the graphite which shifts the CV reduction peak potential from −1.0 V to −0.65 V [54]. The result is increased performance and a reduction in the fraction of current directed toward hydrogen evolution. Kim et al. performed surface reactions on pristine graphite felt resulting in N and O functional groups with high site densities [55]. The modified graphite felt surface increases vanadium redox kinetics by one, to several orders of magnitude. The addition of N functional groups compared to electrodes doped with only O functional groups is greater energy efficiency, reaction kinetics, and initial charge/discharge capability due to reduced overpotential. Huang et al. demonstrated a carbon felt electrode treated with N_2 and O_2 plasma for use in an all-vanadium RFB [56]. The modified electrode resulted in improved electrocatalytic activity and energy efficiency. The test cell performed with an energy efficiency of 78 % at 50 mA cm^{-2}.

Jing et al. added CeO_2 nanoparticles to electrospun carbon nanofibers, shown in Fig. 4(c) to increase the hydrophilicity of the electrode [57]. The modified electrode was found to improve electrocatalytic activity for the anode reaction and increase the electrochemical surface area by four times that of the unmodified electrospun carbon nanofibers, due to the wettability of CeO_2 nanoparticles. Jiang et al. explored the catalytic effect of B_4C nanoparticles on graphite felt in an all-vanadium RFB [58]. They found that the B_4C nanoparticles improve redox reactions due to the abundant unpaired electrons surrounding the central carbon atom. Jiang et al. measured an energy efficiency of 88.9 % at 80 mA cm^{-2} using the modified graphite felt [58]. Zhang et al. synthesized an electrode for use in an all-vanadium RFB using cotton through a pyrolysis process [59]. They found that the carbonized cotton, shown in Fig. 4(d), has a higher surface area, more oxygen-containing functional groups, improved wettability, and higher activity towards vanadium reactions when compared to commercial carbon papers. Zhang et al. achieved an energy efficiency of 74 % at 100 mA cm^{-2} [59].

Overall, the greatest energy efficiency measured in an all-vanadium RFB through electrode modification was done by González et al. using a graphene-modified graphite felt electrode. The energy efficiency was measured to be 95.8 % at 25 mA cm^{-2} [22]. The greatest current density through electrode modification was obtained by Wei et al. using a copper nanoparticle coated graphite felt electrode. A current density of 300 mA cm^{-2} was measured [50].

3.1.3. Membrane modification

Due to crossover of the active species through the ion-exchange membrane, which reduces coulombic efficiency, energy storage capacity, and may result in unwanted side reactions, many researchers have explored the modification of traditional membranes or fabrication of new membranes. Sun et al. studied the effects of self-discharge in a vanadium flow battery [62]. They found that the order of decreasing diffusion for vanadium ions is $V^{2+} > VO^{2+} > VO_2^+ > V^{3+}$ [62]. They also found that when allowing the cell to self-discharge, with continuous flow, five regions result. Each region corresponds with a specific range of open-circuit potential (OCP). Two regions mark the disappearance of a vanadium ion species and result in a rapid drop in OCP [62]. Zhou et al. tested and compared the commercial membrane VANADion, a composite consisting of a porous layer and a dense Nafion layer, against the traditionally used Nafion 115 in an all-vanadium RFB [63]. They achieved an energy density of 76.2 % at 240 mA cm^{-2} using the VANADion membrane, which is estimated to be cheaper than Nafion 115 for mass production [63].

Zeng et al. developed a semi-interpenetrating polymer network consisting of cross-linked polyvinylpyrrolidone and polysulfone for use in an all-vanadium RFB [64]. The membrane exhibited a coulombic efficiency of nearly 100 % at 100 mA cm^{-2}; 3 % higher than Nafion 212 [64]. Yuan et al. developed an aromatic poly (ether sulfone) composite ion exchange membrane to be used in an all-vanadium RFB [65]. They were able to achieve an energy efficiency of 81.61 % (coulombic efficiency of 99.36 %) at a current density of 140 mA cm^{-2} [65]. Luo et al. fabricated a porous poly(benzimidazole) membrane for use in an all-vanadium RFB [66]. This membrane exhibited an energy efficiency of ~87 % (coulombic efficiency of 98 %) at a current density of 40 mA cm^{-2}, 10 % higher than for Nafion 112 [66]. Xia et al. developed a covalently cross-linked sulfonated polybenzimidazole (CSOPBI) membrane for use in an all-vanadium RFB [67]. The membrane has a vanadium permeability that is 3–4 orders of magnitude lower than Nafion 117 and higher coulombic efficiency. The all-vanadium RFB achieved an energy efficiency of ~85 % (coulombic efficiency ~98 %) at 60 mA cm^{-2} with little capacity decay in 300 charge/discharge cycles [67].

Chen et al. fabricated sulfonated poly(phthalazine ether ketone)s containing pendant phenyl moieties (SPPEK-Ps) for use in an all-vanadium RFB [68]. The membranes exhibited lower vanadium ion permeability compared to Nafion 115 (2.53×10^{-5} cm min^{-1} and 9.0×10^{-4} cm min^{-1}, respectively). The all-vanadium RFB achieved an energy efficiency of 83 % (coulombic efficiency 98 %) at 60 mA cm^{-2}, comparable to Nafion 115 [68]. Largier et al. examined the effect of quaternary ammonium homopolymer and ionic/non-ionic random unit copolymerization of Diels-Alder poly(phenylene) copolymers for use in an all-vanadium RFB [69]. The membrane showed a 7 % increase in energy efficiency, ~68 % (~90 % coulombic efficiency), compared to materials of similar ion content at 10 mA cm^{-2} [69]. Ji et al. fabricated sulfonated poly(ether ether ketone)/titanium oxide composite membranes for use in an all-vanadium RFB [70]. With this membrane, the all-vanadium RFB achieved an energy efficiency of 82.9 % (coulombic efficiency of 98.3 %) at a current density of 50 mA cm^{-2}, and selectivity was increased 13 times when compared to Nafion 117 [70].

Wu et al. developed a polysulfone-polyvinylpyrrolidone membrane with a graphene oxide loading for use in an all-vanadium RFB [71]. This membrane exhibited an energy efficiency of 87 % (coulombic efficiency of 98 %) at 60 mA cm^{-2} [71]. Kim et al. developed a composite membrane using sulfonated poly(ether ether ketone) (SPEEK) and finely ground microporous G-AMH-3 [72]. An energy efficiency of ~88 % at a current density of 40 mA cm^{-2} was achieved using the composite membrane [72]. Sadhasivam et al. fabricated a sulfonated poly(phenylene oxide) and nano sized sulfonated silica hybrid membrane for use in an all-vanadium RFB [73]. The hybrid membrane achieved a VO^{2+} crossover rate of 0.173 mmol L^{-1} compared to 14.88 mmol L^{-1} for Nafion 212 [73].

Many researchers have turned their focus to using and improving

anion exchange membranes (AEMs) due to their superior resistance to crossover of the positively charged vanadium ions. However, the supporting (balancing) ion must now be negatively charged, typically resulting in lower ionic conductivity in the electrolyte and ion-exchange membrane. Cha et al. developed a polysulfone-based crosslinked AEM for use in an all-vanadium RFB [74]. The AEM has a much lower ion permeability compared to Nafion 115 (2.72×10^{-8} cm^2 min^{-1} and 2.88×10^{-6} cm^2 min^{-1}, respectively). The all-vanadium RFB with the polysulfone-based crosslinked AEM achieved an energy efficiency of ~86 % (coulombic efficiency of 100 %) after 100 cycles at a current density of 50 mA cm^{-2} [74]. Zhang et al. developed a quaternized adamantane-containing poly(aryl ether ketone) anion exchange membrane (QADMPEK) for use in an all-vanadium RFB [75]. They found that the QADMPEK membrane exhibited low water uptake and significantly lower permeability compared to Nafion 117. An all-vanadium RFB cell using the QADMPEK membrane had an energy efficiency of 84 % (coulombic efficiency 99.4 %) at a current density of 80 mA cm^{-2} [75].

Zeng et al. fabricated a pyridinium-functionalized cross-linked AEM for use in an all-vanadium RFB [23]. The AEM exhibits superior chemical stability and was shown to retain 80 % of its discharge capacity over 537 cycles. The all-vanadium RFB achieved an energy efficiency of ~91 % at a current density of 100 mA cm^{-2} [23]. Yun et al. prepared a functionalized organic/inorganic composite AEM for use in an all-vanadium RFB [76]. The prepared membrane exhibited a coulombic efficiency of 99 % at a current density of 100 mA cm^{-2}, compared to 95 % for Nafion 212. Yun et al. reported an energy efficiency of ~82 % at 100 mA cm^{-2} [76]. Zhang et al. fabricated a poly(phenyl sulfone) AEM with pyridinium groups (PyPPSU) for use in an all-vanadium RFB. The PyPPSU membrane has a lower vanadium ion permeability compared to Nafion 117 resulting in an all-vanadium RFB with an energy efficiency of 80.2 % at 100 mA cm^{-2} (coulombic efficiency 97.8 % compared to 96.1 % for Nafion 117) [77].

Overall, the pyridinium-functionalized cross-linked anion exchange membrane developed by Zeng et al. had the highest energy efficiency of all other membranes reviewed with a measured value of ~91 % at a current density of 100 mA cm^{-2} [23]. The VANADion membrane that Zhou et al. tested supported the highest current density of all membranes with a value of 240 mA cm^{-2} [63].

3.2. Iron-vanadium

In the iron-vanadium RFB the V^{2+}/V^{3+} couple is used as the anolyte active species while the Fe^{2+}/Fe^{3+} couple is used in the catholyte. Souentie et al. tested an iron-vanadium RFB and achieved an energy efficiency of ~72 % with a current density of 51 mA cm^{-2} [78]. They found that the reaction process is controlled by the sluggish V^{2+}/V^{3+} reaction. Due to the cost of vanadium, replacing one of the vanadium redox couples with an inexpensive chemical can significantly reduce the cost of the RFB.

$$Fe^{3+} + e^- \rightleftharpoons Fe^{2+} \qquad 0.771 \text{ V vs.SHE} \tag{3}$$

To combat issues related to crossover in an iron-vanadium RFB, Lee et al. developed an HCl doped meta-polybenzimidazole (m-PBI) membrane [79]. When this membrane is in contact with sulfuric acid, the PBI becomes protonated, which repels cations, exhibiting low crossover and high coulombic efficiency [79]. The PBI based membrane resulted in a higher coulombic efficiency and maintained a higher discharge capacity compared to a Nafion membrane [79]. Unfortunately, energy efficiency is only 70 % at 80 mA cm^{-2}, like Nafion, due to lower conductivity resulting in lower voltage efficiency [79]. The ability of the PBI based membrane to maintain capacity while cycling is promising as this indicates a lower rate of crossover. In RFBs containing different redox species in each half-cell, crossover is an important issue. Improvement of the PBI based membranes conductivity may lead to a very promising material in many different RFB embodiments.

3.3. Iron-chromium

The iron-chromium RFB utilizes the Cr^{2+}/Cr^{3+} redox couple in the anolyte and the Fe^{2+}/Fe^{3+} redox couple in the catholyte. This RFB chemistry was sought out due to the low cost of the active materials. Zeng et al. designed an iron-chromium RFB using a serpentine flow-field to improve performance [80]. The flow battery demonstrated an energy efficiency of 76.3 % at 120 mA cm^{-2} and 79.6 % at 200 mA cm^{-2} [80]. The cyclability of this iron-chromium RFB at 160 mA cm^{-2} is shown in Fig. 5(a). Zeng et al. also designed an interdigitated flow-field for the iron-chromium battery [81]. With the interdigitated flow-field, the iron-chromium battery achieved an energy efficiency of 80.7 % at 320 mA cm^{-2} [81].

$$Cr^{3+} + e^- \rightleftharpoons Cr^{2+} \qquad -0.407 \text{ V vs.SHE} \tag{4}$$

Graphite felt is the standard electrode material chosen for the iron-chromium RFB; however, unmodified graphite felt is hydrophobic, leading to poor electrolyte wetting which effectively limits the reaction surface area, and low electrochemical activity to the Cr^{2+}/Cr^{3+} redox couple. To combat that issue, Chen et al. developed an SiO_2 decorated graphite felt using silicic acid etching [85]. The etching treatment forms pores in the graphite felt, resulting in an increased surface area. The SiO_2 decorated surface increases the number of oxygen functional groups, improving wettability and electrochemical activity. Chen et al. obtained an energy efficiency of 79.66 % at a current density of 120 mA cm^{-2} [85]. Robb et al. sought to improve the capability of the iron-chromium RFB, increasing the operating voltage and improving kinetics by chelating chromium with ethylenediaminetetraacetic acid (EDTA) [86]. The chelated chromium in the iron-chromium RFB resulted in a OCP of 1.62 V and achieved an energy efficiency of 78.1 % at a current density of 0.1 mA cm^{-2} [86]. The reported current density; however, is too low for use in grid energy storage.

3.4. Iodine-sulfur

Li et al. fabricated a polysulfide/iodide RFB, displayed in Fig. 1(c) in the introduction, to achieve a high energy density (43.1 W h L^{-1}, based on catholyte and anolyte volume) [3]. This battery employs the S^{2-}/S_2^{2-} couple in the anolyte and the I^-/I_3^- couple in the catholyte. The RFB exhibited an energy efficiency of 73.01 % at a current density of 15 mA cm^{-2} and offers cost savings ($85.4 kW h^{-1} active materials cost) when compared to traditional vanadium systems ($152.0 kW h^{-1} active materials cost) [3]. During testing, the SOC was kept below 80 % which allowed for higher coulombic efficiency and capacity retention [3,86]. It was found, through UV–vis spectroscopy, that iodine was present [3]. Iodine is a disproportionation reaction resulting from triiodide. This is a source of capacity loss that is more pronounced at a higher SOC. A forced limitation on the available SOC is undesirable as it results in a large portion of essentially unusable electrolyte. In addition, the polysulfide ions can be oxidized to form long-chain, insoluble, polysulfide ions [3]. This is a significant failure mode in the polysulfide/iodide RFB. Even so, the low-cost redox species and high energy density are promising and justify further research. Recently, Rahimi et al. investigated using magnetic modified multiwalled carbon nanotubes to improve the performance of a polysulfide/iodide RFB [87]. They dispersed these nanotubes in the positive electrolyte of the RFB, improving the electrochemical activity [87]. Using the nanotubes, an energy efficiency of 79.9 % at a current density of 20 mA cm^{-2} was obtained [87].

$$I_3^- + 2e^- \rightleftharpoons 3I^- \qquad 0.536 \text{ V vs.SHE} \tag{5}$$

$$S_2^{2-} + 2e^- \rightleftharpoons 2S^{2-} \qquad -0.51 \text{ V vs.SHE} \tag{6}$$

3.5. Cobalt-tungsten

Liu et al. researched the use of a tungsten-cobalt heteropolyacid,

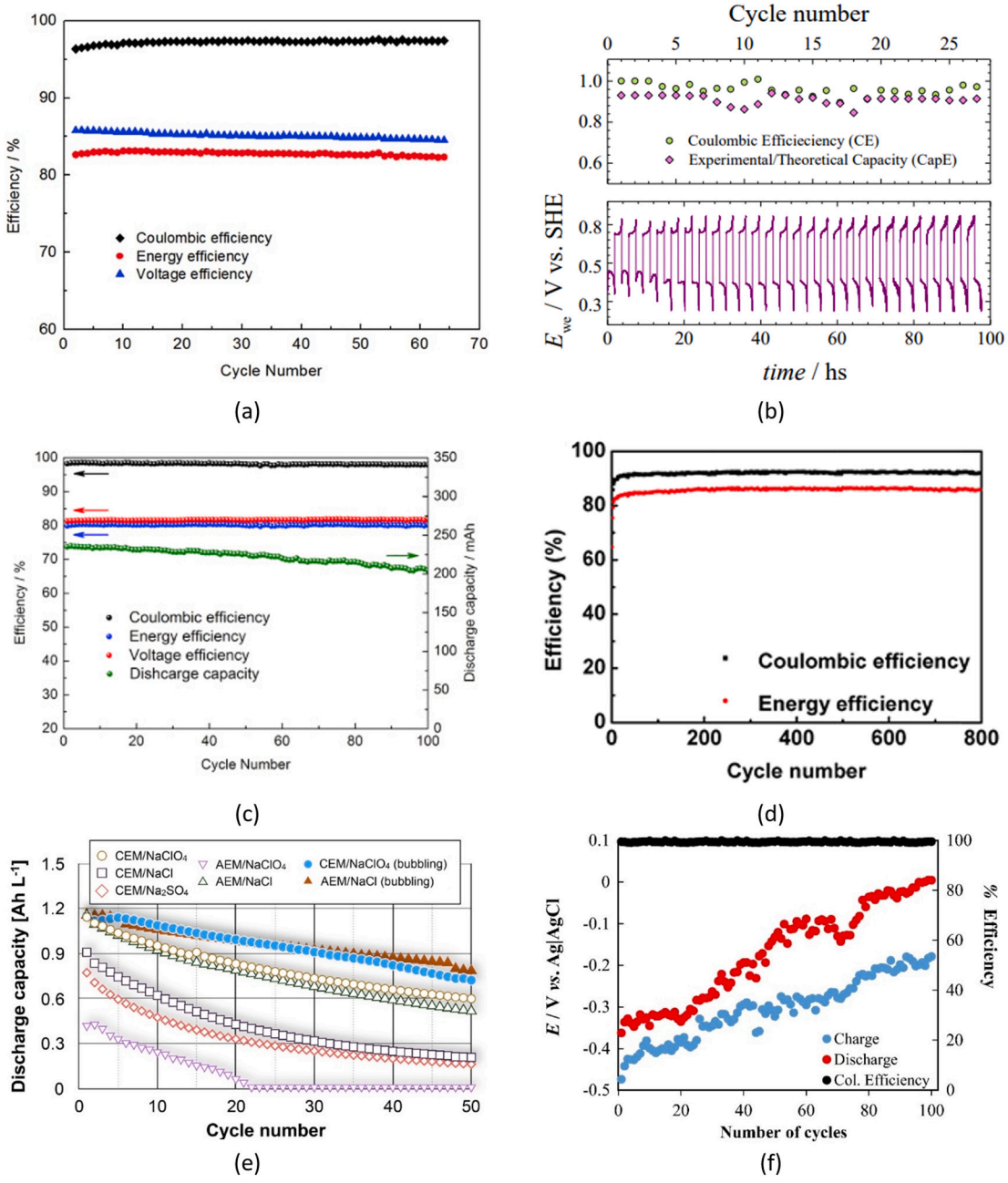

Fig. 5. Cycling performance metrics for (a) an iron-chromium RFB at a current density of 160 mA cm^{-2}, (b) a manganese half-cell RFB, (c) an iron-cadmium RFB, (d) a cerium-lead RFB at a high number of cycles, (e) a zinc-TEMPOL RFB showing different combinations of separators and supporting electrolytes, and (f) a cyclohexanedione half-cell [28,35,80,82–84].

$H_6[CoW_{12}O_{40}]$, as the anolyte and catholyte (mixed electrolyte) in a RFB [88]. Using the same electrolyte on both sides of the battery resolves the issue of irreversible cross contamination that results in permanent capacity loss. In an aqueous solution, the molecule dissociates as a strong acid so, it does not require a supporting solvent. The large size of the $[CoW_{12}O_{40}]$ molecule and its negative charge make it difficult to cross a Nafion membrane, resulting in low crossover and increased columbic efficiency. Thinner membranes can also be used due to less risk of crossover; there is a minimum thickness as ion permeability increases as membrane thickness decreases [89]. The tungsten-cobalt heteropolyacid RFB achieved a specific energy of 15.4 W h L^{-1} and an energy efficiency of 86 % maintained over 30 cycles at a current density of 25 mA cm^{-2} [88].

$$CoW_{12}O_{40}^{5-} + e^- \rightleftharpoons CoW_{12}O_{40}^{6-} \qquad 1.103 \text{ V vs.SHE} \qquad (7)$$

$$CoW_{12}O_{40}^{6-} + 2e^- + 2H^+ \rightleftharpoons H_2CoW_{12}O_{40}^{6-} \qquad -0.074 \text{ V vs.SHE} \qquad (8)$$

$$H_2CoW_{12}O_{40}^{6-} + 2e^- + 2H^+ \rightleftharpoons H_4CoW_{12}O_{40}^{6-} \qquad -0.191 \text{ V vs.SHE} \qquad (9)$$

3.6. Manganese (half-cell)

Colli et al. demonstrated the use of a permanganate redox couple MnO_4^-/MnO_4^{2-} in an alkaline solution as the cathode of a half-cell experiment [84]. This redox couple offers good reversibility and potential for a large energy storage capacity, theoretically 97 A h L^{-1} [84]. They were able to achieve an average coulombic efficiency of 95 % at 100 mA cm^{-2} with a capacity retention of 97 % after 27 cycles, Fig. 5(b)

[84]. The manganese half-cell was cycled against an electrolyte solution containing only the supporting electrolyte, NaOH, which produced hydrogen and oxygen during cycling. Precipitation of MnO_2 remains a problem for the manganese redox couple. Crossover of the manganese ion was observed, and degradation of the reference electrode resulted in lower discharge potentials at higher cycle numbers. To avoid precipitation of MnO_2, the voltage window must be carefully selected. In addition, it was found that the selection of tube plastic and composite carbon materials influenced the rate of MnO_2 precipitation.

$$MnO_4^- + e^- \rightleftharpoons MnO_4^{2-} \qquad 0.558\ \text{V vs.SHE} \qquad (10)$$

3.7. Ferri/ferrocyanide (half-cell)

The ferri/ferrocyanide symmetric cell uses the same electrolyte for the anolyte and catholyte, which takes advantage of the $Fe(CN_6)^{3-}$/$Fe(CN_6)^{4-}$ oxidation states. This redox couple is low cost, stable, and non-toxic [90]. Luo et al. examined the pH dependence of the ferri/ferrocyanide redox flow battery and determined the redox couple has outstanding electrochemical stability under neutral and near neutral conditions [90]. The capacity retention of the symmetric cell was nearly 100 % for all conditions [90]. Luo et al. found that any capacity fade observed was a result of decomposition of the $K_4[Fe(CN)_6]$ catholyte due to the OH^- ion acting as a strong nucleophile [90].

3.8. Vanadium-cobalt

Recently, a novel redox flow battery, utilizing the V^{2+}/V^{3+} redox couple in the anolyte and the Co^{2+}/Co^{3+} redox couple in the catholyte, was designed and tested by Kocyigit et. Al [91]. They tested different concentrations of sulfuric acid and the redox couples for both the anolyte and the catholyte, finding that 4.0 M sulfuric acid was the optimal concentration [91]. It was observed that the battery achieved a cell potential of 2.35 V during charging and had a maximum discharge capacity of 430.1 mAh [91].

3.9. Summary, all-liquid RFB

Table 1 summarizes the values discussed above for various all-liquid RFB systems, while Table 2 gives a comparison of the advantages, disadvantages and research direction/opportunities for the various RFB systems. As is evident from Table 1, the current research space is dominated by the all-vanadium RFB. Data for the all-vanadium RFB from Table 1, along with additional data points from published literature in the years between 2015 and 2020, are plotted and shown in Fig. 6. This figure makes clear the relationship between energy efficiency and current density. As researchers attempt to increase the operating current density, efficiency falters. The vast majority of research is still being conducted below 100 mA cm^{-2}. To improve power density, reducing the electrochemical cell size, current density must be improved while maintaining energy efficiency. Reducing the required cell size reduces capital cost by requiring less ion-exchange membrane material to obtain the same power output. Some research has shown efficiencies above 90 %. Other redox couples have been demonstrated with varying success; however, several issues arise due to crossover, unwanted side reactions, low capacity retention, and/or poor energy efficiency.

Table 1
Theoretical cell voltage, energy efficiency and current density of all-liquid RFBs.

RFB type	Theoretical cell voltage (V)	Energy efficiency (%)	Current density (mA cm^{-2})	Reference
All-vanadium	1.25	68	10	[69]
All-vanadium	1.25	95.8	25	[22]
All-vanadium	1.25	85	40	[51]
All-vanadium	1.25	87	40	[66]
All-vanadium	1.25	88	40	[72]
All-vanadium	1.25	78	50	[56]
All-vanadium	1.25	82.9	50	[70]
All-vanadium	1.25	83.1	50	[48]
All-vanadium	1.25	86	50	[74]
All-vanadium	1.25	83	60	[68]
All-vanadium	1.25	85	60	[67]
All-vanadium	1.25	87	60	[71]
All-vanadium	1.25	76	80	[49]
All-vanadium	1.25	84	80	[75]
All-vanadium	1.25	88.9	80	[58]
All-vanadium	1.25	74	100	[59]
All-vanadium	1.25	80.2	100	[75]
All-vanadium	1.25	82	100	[76]
All-vanadium	1.25	84.8	100	[53]
All-vanadium	1.25	91	100	[23]
All-vanadium	1.25	81.61	140	[65]
All-vanadium	1.25	76.2	240	[63]
All-vanadium	1.25	80.1	300	[50]
All-vanadium	1.25	74.2	320	[43]
Iron-vanadium	1.03	72	51	[78]
Iron-chromium	1.18	76.3	120	[80]
Iron-chromium	1.18	79.6	200	[80]
Iodine-polysulfide	1.05	73	15	[3]
Cobalt-tungsten	1.29	86	25	[88]

4. Hybrid redox flow batteries

4.1. All-copper

In recent years, new chemistries and configurations for the hybrid RFB have been increasingly researched. The reason for such interest is the cost savings offered by redox couples that undergo electrodeposition and the possibility of increasing energy density. In the all-copper RFB, the anolyte uses the Cu^0/Cu^+ redox couple and the catholyte uses the Cu^+/Cu^{2+} redox couple. Lloyd et al. designed an all-copper RFB, with an OCP of 0.65 V, focusing on cost effectiveness, scalability, and energy efficiency [26]. They achieved an energy efficiency of 72 % at a current density of 40 mA cm^{-2} [26]. Leung et al. evaluated electrode materials for use in all copper flow batteries, shown in Fig. 1(d) in the introduction [2]. When using copper fibers as the anode and carbon felt as the cathode they achieved 60 % voltage efficiency and 99 % coulombic efficiency at a current density of 50 mA cm^{-2} over 35 cycles [2]. Sanz et al. explored different supporting electrolytes for the catholyte in an all-copper RFB [112]. They were able to achieve a copper chloride

Table 2
Comparison of the advantages and disadvantages of aqueous RFB systems.

RFB	Strength	Weakness	Opportunities	Ref
All-vanadium	- low irreversible crossover due to using same electrolyte - limited operating range due to precipitation of V2O5 at higher temperatures	-Electrolyte imbalance -contaminations -cell components corrosions -low kinetics constants of active species	- enhanced electrodes, new ion-exchange membranes, and improved cell designs	[44]
Iron-vanadium	- low self-discharge	-significant irreversible crossover -low energy efficiency -High cost of Vanadium	- membranes with low crossover	[78]
Iron-chromium	- low cost of active materials - current density, too low for grid storage	- cross-contamination of the anolyte and catholyte -poor wettability of graphite electrode -operates at high temperature	-improve wettability of electrode -Introducing chelating agents to reduce electrolyte crossover	[81]
Iodine-sulfur	- very low cost redox species - high energy density	- loss of active species to polysulfide/ iodide formation	- methods to promote electrochemical activity	[3,87]
Cobalt-tungsten	- no irreversible crossover due to using same electrolyte - high columbic efficiency	- does not require supporting electrolyte	-improve energy efficiency	[88]

solubility of 3 M with 3 M hydrochloric acid and 4 M calcium chloride, which puts the energy density in the range of 20 W h L^{-1} [112].

$$Cu^{+} + e^{-} \rightleftharpoons Cu \qquad 0.521 \text{ V vs.SHE} \qquad (11)$$

$$Cu^{+} + e^{-} \rightleftharpoons Cu^{2+} \qquad 0.153 \text{ V vs.SHE} \qquad (12)$$

4.2. Copper-iron

Hoyt et al. explored the copper-iron RFB to improve on the plating utilization of copper on a carbon felt electrode [60]. The copper-iron RFB utilizes the Cu^0/Cu^+ redox couple in the anolyte and the Fe^{2+}/Fe^{3+} redox couple in the catholyte giving an OCP of 0.46 V. A single, mixed electrolyte was used for both anolyte and catholyte to reduce concentration-based crossover of the ion-exchange membrane. Hoyt et al. also developed a model to determine plating utilization based on current density and electrode thickness. When electroplating occurs, shown in Fig. 4(e), in Section 3.1.2., Electrode Modification, the plating volume and plating utilization become the upper limit for stored energy. Including 1 M H_2SO_4 into the electrolyte was shown to improve plating utilization by increasing ionic conductivity, compared to an electrolyte without acid [60]. It was also shown that the applied current density has a large effect on plating utilization, which is attributed to the altered current distribution.

4.3. Iron-cadmium

The iron-cadmium RFB employs the Cd^0/Cd^{2+} redox couple in the anolyte and the Fe^{2+}/Fe^{3+} redox couple in the catholyte. Zeng et al. developed an iron-cadmium RFB, with a mixed reactant electrolyte, that achieved an energy efficiency of 80.2 % at 120 mA cm^{-2} [28]. A mixed electrolyte, 1.0 M $FeCl_2$ and 0.5 M $CdSO_4$ in 3.0 M HCl, reduces issues of crossover by reducing the severe concentration gradient, like the copper-iron RFB of Hoyt et al., that occurs with different anolyte and catholyte compositions. The capacity fade seen in Fig. 5(c), located in Section 3.3, is a result of metallic cadmium deposition on the boundary interface between separator and electrode, blocking the ability of the RFB to charge [28].

$$Cd^{2+} + 2e^{-} \rightleftharpoons Cd \qquad -0.40 \text{ V vs.SHE} \qquad (13)$$

4.4. Lead-iron

Zeng et al. demonstrated a working lead-iron RFB that utilizes the Fe^{2+}/Fe^{3+} and Pb^0/Pb^{2+} redox couples [113]. This redox chemistry was selected to create a low-cost RFB without the low redox potential of a vanadium anolyte couple, to avoid hydrogen evolution. The RFB achieved an energy efficiency of 86.2 % (coulombic efficiency of 96.2 %) at a current density of 40 mA cm^{-2} [113]. The coulombic and energy efficiency of the lead-iron RFB is shown in Fig. 5(d), located in Section 3.3, with a high number of cycles.

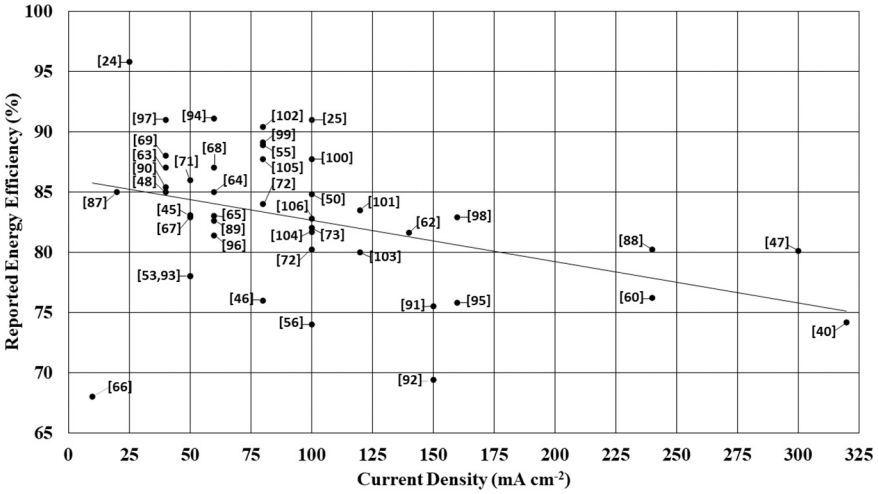

Fig. 6. Energy efficiency vs. current density reported in literature for the all-vanadium RFB [92–111].

$$Pb^{2+} + 2e^- \rightleftharpoons Pb \qquad -0.13 \text{ V vs.SHE} \qquad (14)$$

4.5. Cerium-lead

Na et al. developed a cerium-lead RFB using methanesulfonic acid as the supporting electrolyte and achieved an energy efficiency of 86 % over 800 cycles with a coulombic efficiency of 92 % at a current density of 5 mA cm^{-2} [83]. The cerium-lead RFB utilizes the Pb^0/Pb^{2+} redox couple in the anolyte and the Ce^{3+}/Ce^{4+} redox couple in the catholyte. This chemistry offers high redox potential from cerium, which increases power density, and an anolyte that suppresses hydrogen evolution.

$$Ce^{4+} + e^- \rightleftharpoons Ce^{3+} \qquad 1.72 \text{ V vs.SHE} \qquad (15)$$

4.6. All-lead

Krishna et al. examined the electrolyte properties of a soluble lead acid RFB which uses the Pb^0/Pb^{2+} redox couple in the anolyte and the Pb^{2+}/Pb^{4+} redox couple in the catholyte [114]. They achieved a voltage efficiency of 72 % and a coulombic efficiency of 81 % at a current density of 15 mA cm^{-2} [114]. A low-cost supply chain exists for this redox chemistry from the established industry of recycling conventional lead acid batteries. Soluble lead acid RFBs are plagued by lead dendrites that form on the anode [115]. Recently, Rathod et al. found the use of sodium lignosulfonate and sodium fluoride electrolyte additives in the RFB improved the cycle-life and reduced the lead deposits on the electrodes [115].

$$PbO_2 + 4H^+ + 2e^- \rightleftharpoons Pb^{2+} + 2H_2O \qquad 1.455 \text{ V vs.SHE} \qquad (16)$$

4.7. Iron-zinc

Selverston et al. tested an iron-zinc RFB using a mixed electrolyte in a NH_4Cl supporting electrolyte [116]. The iron-zinc RFB uses the Zn^0/Zn^{2+} redox couple in the anolyte and the Fe^{2+}/Fe^{3+} redox couple in the catholyte. Selverston et al. found that iron plating is inhibited by the presence of Zn^{2+} and zinc ions have no significant effect on the catholyte. This system could employ a cheap, compared to Nafion, microporous separator. The system maintained an OCP of 1.5 V and remained stable after 10 days of 100 continuous cycles [116]. The coulombic, voltaic, and energy efficiencies were 85 %, 80 %, and 68 %, respectively, at a current density of 25 mA cm^{-2} [116].

$$Zn^{2+} + 2e^- \rightleftharpoons Zn \qquad -0.76 \text{ V vs.SHE} \qquad (17)$$

4.8. Iodine-zinc

Li et al. demonstrated an iodine-zinc RFB with an energy of 167 Wh l^{-1} using a 5 M ZnI_2 electrolyte at near neutral pH [117]. The anolyte redox couple is Zn^0/Zn^{2+} and the catholyte redox couple is I_3^-/I^-. The addition of ethanol was tested which expanded the electrolyte's stable temperature window to −20–50 °C and ameliorated zinc dendrite formation [117]. ZnI_2 salt was dissolved in water to act as a mixed anolyte and catholyte. The use of iodine-zinc RFBs is affected by the high cost of ZnI_2, their low energy and voltage efficiencies along with their poor stability [118]. To address these issues, Mousavi et al. created a low-cost ammonium chloride supported iodine-zinc RFB that used the ammonium iodide/triiodide redox couple [118]. They found that this setup reduced zinc dendrites at the anode, improved cycle life and improved energy efficiency [118].

4.9. Zinc-bromine

The zinc-bromine RFB employs the Zn^0/Zn^{2+} redox couple in the anolyte and Br_2/Br^- redox couple in the catholyte. Yang et al. explored the effects of electrolyte flow rate on the formation of zinc dendrites in a zinc/bromine RFB [119]. They found that poor mixing of the polybromide and aqueous phase (partially dependent on electrolyte flow rate) resulted in increased zinc dendrite formation in the anode. Wu et al. investigated the use of KCl and NH_4Cl to improve the conductivity of the electrolyte in a zinc-bromine RFB [120]. They found that using 4 M NH_4Cl as a supporting electrolyte allows for the operation of the battery at a current density of 40 mA cm^{-2} while maintaining an energy efficiency of 74.3 % [120]. Energy efficiency can be further improved by thermal treatment of the graphite felt electrode, up to 81.8 % [120]. Yang et al. introduced a surface active agent, polyoxyethylene(20)sorbitan monolaurate, to improve the stability and coulombic efficiency in a zinc/bromine RFB [121]. They found that the addition of the surface-active agent enhanced mixing of the polybromide-complex phase allowing coulombic efficiency to remain stable over 30 cycles.

$$Br_2(aq) + 2e^- \rightleftharpoons 2Br^- \qquad 1.07 \text{ V vs.SHE} \qquad (18)$$

Zinc-Bromine RFB offers the advantages of high cycle life, low cost materials, and full discharge capability; but are limited by their expensive complexing agents needed to mitigate emission of toxic Bromine vapor and dendrites formation if not discharged frequently [122].

4.10. Zinc-cerium

Chen et al. demonstrated an aqueous ionic liquid electrolyte, 1-butyl-3-methylimidazolium chloride (BMImCl)-H_2O, used in the in a hybrid zinc-cerium RFB [123]. The zinc-cerium RFB uses the Zn^0/Zn^{2+} redox couple in the anolyte and the Ce^{3+}/Ce^{4+} redox couple in the catholyte. In this system, BMImCl offers high stability against hydrolysis, allowing an expanded electrochemical window of 3 V. In addition, the chlorine ion from BMImCl can act as the charge carrier with the use of an AEM. Arenas et al. tested different platinum/titanium electrode structures (plate, micromesh, and felt) for use in a zinc-cerium hybrid RFB [124]. They found that platinized-titanium micromesh is a more effective electrode material and titanium felt with high platinum coverage has the best volumetric mass transport characteristics. Testing was performed at low current densities, 0.025 to 0.075 mA cm^{-2}, to reduce the impact of ohmic losses due to the AEM [123]. Recently, Amini et al. utilized polarization and electrochemical impedance spectroscopy to ascertain the causes of voltage loss in zinc-cerium RFBs, whether it be due to kinetic, ohmic or mass transfer overpotentials [125]. They found that kinetic overpotentials in the negative half cell severely contributed to performance loss at low and intermediate current densities, while it was mass transfer limitations in the positive half-cell that affected performance at high current densities [125]. Additionally, they found that a mixed methanesulfonate-chloride negative electrolyte reduced kinetic overpotentials in the negative half-cell and increasing the flow rate in the battery led to increased mass transfer in the positive half-cell [125].

4.11. Cadmium-organic

Yousofian-Varzaneh et al. developed a hybrid RFB based on tetrafluoro-*p*-hydroquinone, $TFQH_2$, and 3-fluorocatechol, $3FQH_2$, as the oxidized cathode species and cadmium electrodeposited from Cd^{2+} onto a copper electrode as the anode reaction [61]. The OCP of this cell was between 1.0 and 1.3 V at a state of charge (SOC) of 98 %. Cadmium was chosen because it has a large negative standard electrode potential but high hydrogen evolution overpotential. Cadmium deposition on a copper electrode is shown in Fig. 4(f), located in Section 3.1.2., Electrode Modification. This hybrid RFB exhibited an energy efficiency of 80 % at 5 mA cm^{-2} with negligible capacity loss.

4.12. Sulfur-air

Li et al. demonstrated an aqueous sulfur and air-breathing RFB with a maximum energy density of 145 Wh L^{-1} [40]. This configuration was chosen because of its low chemical cost compared to other RFBs. The

anolyte is an aqueous polysulfide, S_4^{2-}/S_2^{2-} and the catholyte is an oxygenated salt solution (containing Li^+ or Na^+ ions). During charge the working ions cross the membrane into the anolyte maintaining electroneutrality, while oxygen evolution occurs in the catholyte. The OCP varies depending on the pH of the catholyte. An acidic catholyte gives an OCP of 1.68 V while an alkaline catholyte gives an OCP of 0.85 V [40]. At a current density of 0.325 mA cm^{-2}, Li et al. achieved a voltage efficiency of 55 % [40].

4.13. Hydrogen-bromine

Oh et al. developed a model to simulate the effects of flow field designs on the hydrogen/bromine RFB, shown in Fig. 1(e) in the introduction [1]. The anolyte redox couple was H_2/H^+ and the catholyte redox couple was Br_2/Br^-. The model was validated against an experimental RFB up to a current density of 1 A cm^{-2} [1]. The hydrogen-bromine RFB represents a high energy density and highly reversible solution to RFB technology. In addition, the hydrogen charge/discharge portion of this RFB can utilize existing hydrogen technology and/or advance hydrogen production technology. Researchers such as Karaeyvaz et al., are investigating the use of cathode catalysts to improve the performance of hydrogen-bromine RFBs [126]. In their study, Karaeyvaz et al. synthesized hollow core mesoporous shells of carbon nanomaterials using a process developed for silica and utilized them as a cathode electrocatalyst due to their high electroactive surface area [126]. Using this nanomaterial with a specific surface area of 1832 m^2/g, a power density of 0.50 W/cm^2 at 0.7 V cell potential was obtained, indicating their usefulness in the boosting performance of hydrogen-bromine RFBs [126].

$$2H^+ + 2e^- \rightleftharpoons H_2 \qquad 0.00\ \text{V vs.SHE} \qquad (19)$$

4.14. All-iron

The semi-solid category of RFBs is an emerging field of research with intriguing prospects. The semi-solid RFB, sometimes referred to as semiflow or slurry, uses a network of electrically conductive particles suspended in the anolyte and/or catholyte to act as the electrodes. When the concentration of particles is above some threshold, it forms an electrically conductive network allowing for the transfer of electrons from reaction to a current collector and out of the cell or vice versa. This slurry of electrically conductive particles can flow through the cell introducing fresh particles for reaction. With a redox couple that involves a plating chemistry, the cycling of particles through the cell is the key feature of the semi-solid RFB. The plating reaction can take place on the electrically conductive particles, or electrodes, and be removed from the cell; again, separating power and energy. So, systems that showed promise in safety and cost; but, where prohibited by a plating reaction, are now back on the playing field. Additionally, this flowing network of electrodes can offer increased reaction area compared to stationary electrodes.

Petek et al. developed an all-iron RFB using slurry electrodes, which consisted of multi-walled carbon nanotubes (MWCNTs), to decouple energy storage and power. A > 95 % plating efficiency on the slurry electrode, as opposed to the current collector, was obtained at a current density > 200 mA cm^{-2} [27]. MWCNTs used as the slurry electrode had an outer diameter of 50–80 nm, length of 10–20 μm, and a surface area of 40 m^2/g [27]. The electronic conductivity of the slurry electrode was 85 mS cm^{-1}, while flowing, at a concentration of 4.8 vol% MWCNTs [27]. The catholyte contained 0.5 M $FeCl_2$, 0.5 M $FeCl_3$ (ferric chloride was included to ensure the anolyte was limiting during discharge), and 1.0 M NH_4Cl as the supporting electrolyte. The anolyte contained 0.5 M $FeCl_2$ and 1.0 M NH_4Cl. Both electrolytes had an ionic conductivity of 140 mS cm^{-1} [27]. The reported voltage efficiency is just above 50 %, which means the energy efficiency is lower [27]. The energy efficiency of this system is significantly lower than what is acceptable for grid energy storage.

4.15. Summary, hybrid RFB

Results from studies presented in this work are shown in Table 3. There is a wide variation in the operating cell voltage for hybrid RFBs. In addition, the operating current density and energy efficiency vary significantly. The data from Table 3, along with additional data taken from published literature in the years between 2015 and 2020, are shown in Fig. 7. It is evident from this figure that hybrid RFBs tend to operate at low current densities with lower energy efficiencies than the all-liquid RFBs. Hybrid RFBs represent a low-cost alternative to the all-vanadium RFB. In general, hybrid RFBs require better energy efficiency and operating current density to become competitive in grid energy storage.

5. Organic redox flow batteries

5.1. All-sodium

Senthilkumar et al. developed a sodium catholyte based RFB using NASICON as the ion-exchange membrane [137]. The cell consisted of a Na-metal anode, organic anolyte, NaHCF catholyte, and carbon felt cathode. The organic anolyte consisted of 1 M $NaCF_3SO_3$ in the solvent TEGDME. The catholyte does not require a supporting electrolyte as the sodium ions cross the ion-exchange membrane to balance charge. Senthilkumar et al. achieved a cell potential of 3.06 V (vs Na/Na^+), an energy density of 54.16 W h L^{-1} (catholyte volume), and an energy efficiency of ~92 % at 0.25 mA cm^{-2} [137].

5.2. Zinc-TEMPOL

Orita et al. developed a RFB with a 4-hydroxy-2,2,6,6-tetramethyl-1-pipperidinyloxyl (TEMPOL) catholyte and Zn anolyte [82]. The RFB achieved an energy efficiency of 80.4 % at a current density of 10 mA cm-2 with an open circuit voltage of 1.46 V [82]. The discharge capacity of the zinc-TEMPOL RFB with different combinations of separators and supporting electrolytes is shown in Fig. 5(e), located in Section 3.3. In each iteration capacity fade is a significant issue. Liu et al. developed an RFB using methyl viologen as anolyte, 4-hydroxy-2,2,6,6-tetramethylpiperidin-1-oxyl (4-HO-TEMPO) as catholyte and NaCl as supporting electrolyte. Their system showed a high cell voltage of 1.25 V and 100 % columbic efficiency after 100 cycles while operating between current densities of 20 to 100 mA cm^{-2} [138].

5.3. Cyclohexanedione (half-cell)

Leung et al. examined the use of cyclohexanedione as the anode active species in a RFB [35]. The reduction of 1,3-cyclohexanedione exhibits a potential of −0.6 V vs. Ag|AgCl with an operating range of 1–5 pH. In a half-cell, the reduction and oxidation of 1,3-cyclohexanedione displayed a coulombic efficiency of 99 % at 3.2 mA cm^{-2} [35]. The charge and discharge potential as a function of cycle number is shown in Fig. 5(f), located in Section 3.3, along with the coulombic efficiency. As the cycle number increases, the charge and discharge potential shift to a more positive value.

6. Specialized flow batteries

6.1. Zinc-quinone

To lower RFB costs, Leung et al. tested a membrane-less RFB using the zinc/para-benzoquinone redox couple [24]. The theoretical OCP of the couple varies between 1.17 and 1.59 V depending on the pH. During discharge zinc undergoes dissolution to Zn^{2+} and para-benzoquinone (pBQ) is reduced to hydroquinone (HQ). The challenge of a

Table 3
Theoretical cell voltage, energy efficiency, and current density of hybrid RFBs.

RFB type	Theoretical cell voltage (V)	Energy efficiency (%)	Current density (mA cm^{-2})	Reference
All-copper	0.37	72	40	[26]
All-copper	0.37	59.4	50	[2]
Iron-cadmium	1.17	80.2	120	[28]
Lead-iron	0.9	86.2	40	[113]
Cerium-lead	1.85	86	5	[83]
All-lead	1.58	58.3	15	[114]
Iron-zinc	1.53	68	25	[116]
Zinc-bromine	1.83	81.8	40	[120]

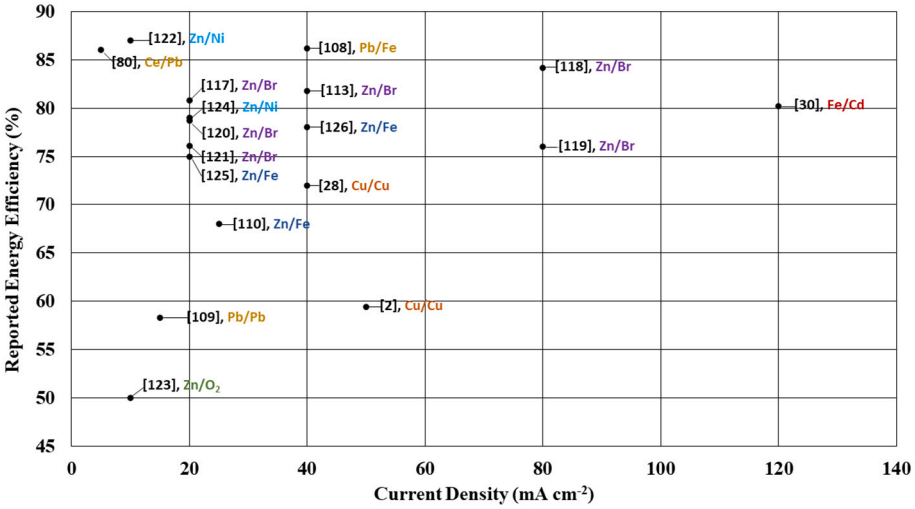

Fig. 7. Energy efficiency vs. current density reported in literature for aqueous, hybrid RFBs using various redox couples [113,120,127–136].

membraneless system is the oxidation of the charged anolyte active species by the charged catholyte active species. Leung et al. controlled this effect by using a low concentration of the hydroquinone species (solubility limit 100 mmol dm^{-3}) [24]. They were able to achieve an energy efficiency of 44.1 % at a current density of 30 mA cm^{-2} [24].

6.2. Concentration gradient

van Egmond et al. explored the use of a concentration gradient in a NaCl solution [39,139]. When fully discharged, the flow battery has two reservoirs containing solutions of the same salinity. During charge, the salinity of one reservoir is increased and the other reduced due to a potential difference applied across an ion exchange membrane. The experimental setup of van Egmond et al., shown in Fig. 3(c), located in Section 3.1.1., Electrochemical Cell Design, resulted in a round trip efficiency of 42 % at 2.5 mA cm^{-2} [39]. Kingsbury et al. developed a concentration gradient flow battery using concentrated and dilute NaCl solutions to produce the gradients [140]. Their flow battery achieved a round-trip efficiency of 34 % at a current density of 1.71 mA cm^{-2} [140].

6.3. Acid-base junction

Kim et al. developed a flow battery, displayed in Fig. 1(f) in the introduction, that exploits the acid-base junction potential instead of reduction-oxidation potential [4]. To achieve this, the flow battery employs two redox compartments, an ion neutralizing compartment, and the acid-base junction. In the redox compartments, oxidation and reduction of iron occurs. The ion neutralizing compartment allows for the transfer of Na^+ and Cl^- to balance the cell. At the acid-base junction, water is split to H^+ and OH^- during charge and recombined during discharge. An energy efficiency of 76 % was obtained at a current density <5 mA cm^{-2}; however, efficiencies quickly decayed after 10 cycles [4].

Sáez et al. developed an acid-base electrochemical flow battery (ABEFB) [141]. During charging of this type of flow battery, hydrogen is oxidized in the cathode (making a concentrated acidic solution) and evolved in the anode (making a concentrated alkaline solution). During discharge, the electrolytes are neutralized, releasing the stored energy. The electrolyte flow must change compartments between charge and discharge to take advantage of the platinized titanium electrode during hydrogen evolution reaction and the platinum-catalysed gas diffusion layer during oxidation (where hydrogen gas is routed). This flow battery achieved an energy efficiency of 55 % at 49 mA cm^{-2} with a coulombic efficiency of 95 % [141].

6.4. Solid charge storage

To address the poor conductivity of insertion materials, Wang et al. proposed the redox targeting reaction mechanism in 2006 to enhance reversible redox reaction using solid energy storage materials, which are both spatially and electrically separated from the current collector [142]. In 2017, Zanzola et al. developed a redox flow battery using a solid charge storage material to increase the energy density of the system [41]. In this system, the solid storage material resides in the electrolyte storage tank and exchanges electrons with a soluble redox mediator, as shown in Fig. 3(d), located in Section 3.1.1., Electrochemical Cell Design. The redox mediator acts as shuttle transferring electrons between the solid storage media and the electrodes of the flow battery. Zanzola et al. examined the use of polyaniline (PANI) as the solid storage material with Fe^{3+}/Fe^{2+} or V^{4+}/V^{3+} as the redox mediators. They found that using Fe^{3+}/Fe^{2+} as the redox mediator allowed for respectable specific capacity (64.8 mA h g^{-1} at 38.5 mA cm^{-2}) and cycling stability over 25 cycles. In the complete flow battery tests, PANI

had to be combined with carbon black, which improved electronic conductivity, to increase the energy storage capacity of the system. Recently, Wong et al. reported a redox-targeting flow battery (RTFBS) wherein a redox-active organic molecule was built into an insoluble polymer to create a shuttle(mediator)- solid(storage) pair. This pairing allowed the RTFB to operate at higher SOCs (>85 %), high polymer utilization (>90 %), and high voltaic efficiencies (>75 %) with a 4-fold increase on storage capacity over conventional RFBs [143].

7. Current research trends and technical issues

Current research in RFBs is focused on three primary areas including chemistry configurations, materials modifications, and cell design. Chemistry configurations refers to the types of redox couples utilized such as the chemical species, reaction type (i.e. plating), organic molecules, catalyst additives, etc. To date, there is no overall best chemistry configuration. The all-vanadium is the current front runner; however, the cost of the active species itself seems to be an insurmountable obstacle based on recent research. In that regard, materials modifications have received a great deal of attention in recent years. Materials modifications primarily focus on the electrode and ion-exchange membrane. These modifications typically allow for incremental improvements in existing systems. In some cases, a significant shift in material may result in a large improvement in cell efficiency, longevity, or capacity retention. Lastly, cell design and/or optimization is an area of focus currently, due to the desire to keep pushing the forward the all-vanadium RFB. Again, these changes typically offer only incremental improvements to existing technologies. However, some research attempts to push the envelope with regard to traditional cell design, offering new hopes.

7.1. Chemistry configurations

A large portion of current research is focused on improving the all-vanadium RFB through cell configuration and enhanced materials. The all-vanadium RFB is well researched so, it is worthwhile and easy to compare results to previous work. However, discoveries and improvements made while working on the all-vanadium RFB will likely have an impact on other chemistry configurations. Different chemistries are continually being explored with the hope of finding a novel breakthrough. Chemistry configuration improvements primarily focus on cost as compared to the all-vanadium RFB; but also, energy density, power density, efficiency, and capacity retention. Energy density is obtained by utilizing chemistry configurations with higher operating potential and better solubility. Power density also results from higher operating potential. Improved operating current density also leads to increased power density. As seen above, higher operating current density often comes at the cost of energy efficiency. Efficiency generally comes from improvements to the ion-exchange membrane but can be significantly affected by the choice of active species and supporting electrolyte. Capacity retention often goes together with efficiency. In some cases, capacity retention is affected by the active species choice, as side reactions can occur, degrading capacity. A comprehensive cost comparison of redox chemistries previously implemented in a RFB, along with other secondary battery materials, is shown in Fig. 8. The all-vanadium RFB is quite high in this fig. A wide range of lower cost redox active species exist. At this point in RFB research, significant cost reductions mainly come from a change in the active redox species to a cheaper soluble metal such as iron. Some cost reductions are also found in using a microporous separator instead of an ion-exchange membrane; however, this typically comes with a loss in efficiency.

A relatively new and promising RFB technology is the slurry electrode. This is promising as it allows for the separation of energy and power while using a cheap electroplating metal as one or both redox couples. The slurry RFB can also provide a greater reaction surface area, increasing operating current density, compared to a stationary

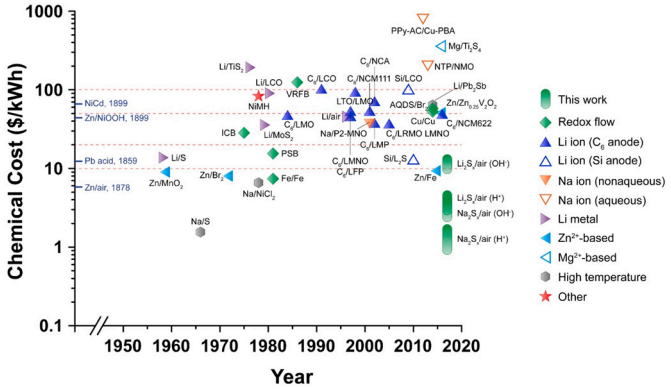

Fig. 8. Chemical cost for a wide variety of RFB chemistries along with some other secondary battery materials [25].

electrode, while increasing voltage efficiency due to decreased diffusion distance. Slurry RFBs; however, suffer from high viscosity when particle loading is increased. A significant particle loading is required to develop a conductive network. There is a difficult tradeoff between electrolyte viscosity and electronic conductivity. Increased loading increases viscosity, requiring more pumping power and/or more expensive pump designs. Decreasing particle loading leads to a prohibitively low electronic conductivity.

Other researchers are currently exploring non-aqueous redox flow batteries. In a 2020 study, Zhen et al. designed and tested an all-iron non-aqueous redox flow battery [144]. Consisting of an iron acetylacetonate anolyte and a Fc1N112-TFSI catholyte, an energy efficiency of 83.4 % at a current density of 10 mA cm^{-2} was obtained over 100 cycles [144]. These results indicate that non-aqueous redox flow batteries are a promising avenue for further investigation.

7.2. Materials modifications

The modification of materials allows for improvement to several key areas of RFBs including reaction kinetics, available surface area, ionic conductivity, cost, and reduced active species crossover. Electrode modification is a hot topic offering incremental improvement to energy efficiency and operating current density. Both graphite felt and carbon paper have been extensively modified through various methods including heat, chemical, and plasma treatment, among others. These modifications improve electrode performance by increasing wettability, reaction kinetics, and surface area. Improvement in wettability allows for more active species to come into contact with the electrode surface, effectively increasing reaction surface area. Improved reaction kinetics can result in improved energy efficiency at higher current density. Higher operating current density is important as it can lead to a reduced system size, lowering overall cost. Increased surface area also leads to improved operating current density while maintaining energy efficiency. In some instances, catalysts have been applied to electrodes; however, catalysts tend to increase gas evolution rates resulting in reduced coulombic efficiency. A 2020 study conducted by Zhang et al. examined the properties and performance of polyacrylonitrile-based graphite felt and carbon felt before and after thermal activation [145]. It was shown that thermally activated graphite and felt electrodes improved energy efficiency in an iron-chromium RFB [145]. Another 2020 study, by Yu et al. aimed to improve existing lead dioxide electrodes through utilizing the properties of lead dioxide' alpha and beta polymorphs [146]. Both polymorphs were electrodeposited on electrodes in methanesulfonate acid [146]. These electrodes were shown to have a longer useful lifetime than existing lead dioxide electrodes [146].

The ion-exchange membrane is a source of significant capital cost in RFBs. Recently, this area of research has increased. Low cost ion-exchange membranes can significantly reduce RFB capital cost,

making the RFB system cost competitive while utilizing more expensive active species like vanadium. Unfortunately, thus far, low cost ion-exchange membranes have not been as effective in limiting crossover while maintaining high ionic conductivity as the traditionally used ion-exchange membrane, Nafion. There is always a significant tradeoff between ionic conductivity, active species crossover, and cost. Reduced ionic conductivity leads to lower energy efficiency through reduced voltage efficiency. Increased active species crossover results in increased capacity fade and may or may not be recoverable. Current research into this area includes Kumar et al. who synthesized a new cross-linked, amphoteric ion-exchange membrane, composed of a sulphonated poly (ether ether ketone) grafted with 2,4,6-tris(dimethylaminomethyl) phenol [101]. This membrane demonstrated high ionic conductivity and low VO^{2+} crossover, indicating its usefulness as a potential membrane in RFBs [101].

7.3. Cell design

Cell and stack design are another research area that has been of interest for some time. At the grid storage level, an RFB stack will contain many cells and large flow plates compared to the laboratory scale. Because of this, research into improving the design of the cell and stack is important to drive down capital costs by reducing material costs, increasing power density, and reducing the required pumping power. Many research groups have moved from the flow-through to the flow-by design, introducing serpentine, interdigitated, or other flow fields. This increases power density and efficiency at the cost of increased pumping power. In addition, material degradation must be examined in certain electrolyte compositions. There is a need for the development of detailed computational models to assist in optimizing RFB design, assist in scale up, and accurately monitor/predict the state of health of an RFB. In addition to circular RFB design, there have been some intriguing novel concepts in recent years. Some of these concepts, the concentration gradient flow battery for instance, utilize the overall flow battery scheme; but, do not include a redox couple. Others utilize some outside of the box thinking to improve on some key aspect of RFBs such as increasing energy density with the solid charge storage RFB. Unlike other technologies, there is much room for innovation in RFB research. One unique design, researched by Kim et al. in 2020, combined a capacitive deionization system with a redox flow battery to effectively desalinate water [147]. The system utilized the RFB's electrolytes to store the salt ions from the capacitive deionization of the water, preventing electrode deterioration in the capacitive deionization system, an issue plaguing the technology [147]. Other researchers have recently analyzed the environmental impact and costs of RFBs. In a 2020 study, Gouveiaa et al. performed a Life Cycle Assessment on a 5 kW vanadium RFB [148]. They found that the battery's cell stack and vanadium electrolytes have the highest environmental impact [148]. Assessing the environmental impact of scaling the battery, they found that storage capacities of 180 kWh and greater were optimal [148]. Xue et al. researched the economics of a zinc-bromine flow battery installed in a microgrid system containing a solar array [149]. Data collected indicated that the flow battery was a major contributor to energy cost savings as it was able to store and distribute excess collected energy [149]. Current research such as these studies, are allowing researchers to clearly assess the advantages of RFB technology and their commercial performance.

To improve efficiency, energy density, power density, and drive down the levelized cost of energy for RFBs, research must identify the following:

1. Low-cost active species with fast reaction kinetics, high solubility, and high operating potential. A compatible catalyst may be necessary to improve reaction kinetics, allowing for a higher operating current density.
2. Electrode materials with improved surface area, high activity towards active species, high corrosion resistance, and high overpotential to gas evolution.
3. Ion-exchange membranes with high ionic conductivity, phenomenal ion selectivity, low cost, and good mechanical strength.
4. Novel stack designs that improve efficiency, power density, reduce pumping losses, and reduce shunt current losses.

7.4. Current problems and solutions for aqueous RFB systems

The all-liquid redox flow batteries are still the most matured of the RFB technology with All-Vanadium RFBs being the most researched and commercialized. The expansion of this technology to meet broad energy demands is limited by the high capital cost, small operating temperature range and low energy density. These limitations can be overcome by developing cost effective electrolytes with higher vanadium solubility, stability and electrochemical performance; low cost separators and improved chemical activity to allow for higher concentrations of Vanadium in order to increase energy densities [150]. Iron –Chromium RFB offers lower capital cost but is strongly challenged by their elevated temperature requirement which leads to higher capacity decay in addition to hydrophobicity of the graphite felt positive electrode which hampers the electrochemical reaction [29]. The solutions to these have been to introduce mixed reactants for both anolyte and catholyte to improve electrochemical performance while reducing crossover rate. Chelation has also been demonstrated to improve the solubility and electrochemical properties of the Fe—Cr RFB [151]. The major challenge of Iodine-Sulfur RFB is the severe shuttling of iodine and polysulphides especially at high SOC, which is a major source of capacity loss. Improving electrochemical performance of the polysulphide/iodide RFB can help mitigate this challenge. One approach to mitigate this is to develop a dual polysulphide-lithium catholyte to alleviate shuttling and passivation [152].

The hybrid RFBs have also received significant industrial investment due to their lower cost and wider potential window, yet they are posed with some significant challenges that must be overcome. The all copper RFBs suffers from permeation of Cu^{2+} species due to crossover effect, solution should explore uniform and reversible electrodeposition of copper to extend the life of the battery in addition to seeking a selective permeable membrane to prevent Cu^{2+} permeation [153]. The Zinc based RFBs: Zn—Fe, Zn – Ce, ZN- Br RFBs, have combined advantages of low cost due to the large abundance of Zn, high voltage and good energy density [154]. Mitigating Zn dendrite formation, preventing hydrogen evolution, and Zinc corrosion are the greatest challenge; some researchers have adopted specialized membrane such as the AEM separator which showed no dendrite formation on the electrode, while others have proposed a membrane-less system [155,156].

The top challenges with the organic RFBs are crossover and capacity fade due to chemical degradation. Crossover can be mitigated by developing advanced ion-exchange membrane with zero crossover tolerance. More research work is needed to improve ionic conductivity, cell voltage and membranes of for organic RFBs.

8. Conclusion

In conclusion, this review highlighted the different areas of redox flow battery research ranging from all-liquid to hybrid to specialized flow batteries. This article also identified trends in the current research and areas for further improvement.

RFBs will play a vital role in the global energy shift towards renewable energy. This type of battery is uniquely suited to meet the requirements of renewable energy storage due to its cost, efficiency, safety, and scalability. RFBs will allow for more robust renewable energy systems that meet the demands of our society. If we are to eliminate our reliance on fossil fuels, technology such as RFBs must be leveraged to their full advantage, starting with research into improving their

design and function. In the case of all-liquid redox flow batteries, more research is needed to improve current density while maintaining optimal energy efficiency. Research into this area will lead to cheaper and smaller all-liquid RFBs in the near future. Hybrid RFBs are a promising, cheaper alternative to all-liquid RFBs, however they require further research to achieve current densities comparable to all-liquid RFBs. Furthermore, research into organic active species for RFBs is also gaining traction. This research will need to ascertain the feasibility of these molecules as they are large and complex. These future research avenues will provide new approaches to improve RFB efficiency, cost, and energy storage capacity, placing them on track to become an essential part of renewable energy storage, paving the way for a cleaner, brighter future.

Declaration of competing interest

The authors declare that they have no known competing financial interests or personal relationships that could have appeared to influence the work reported in this paper. Sam Park reports financial support was provided by University of Louisville.

Data availability

No data was used for the research described in the article.

Acknowledgements

This work was supported by the NSF: IUCRC (EVSTS: # 2147117).

References

[1] K. Oh, et al., Effect of flow-field structure on discharging and charging behavior of hydrogen/bromine redox flow batteries, Electrochim. Acta 230 (Supplement C) (2017) 160–173.
[2] P. Leung, et al., Evaluation of electrode materials for all-copper hybrid flow batteries, J. Power Sources 310 (Supplement C) (2016) 1–11.
[3] Z. Li, et al., A high-energy and low-cost polysulfide/iodide redox flow battery, Nano Energy 30 (Supplement C) (2016) 283–292.
[4] J.-H. Kim, et al., Proof-of-concept experiments of an acid-base junction flow battery by reverse bipolar electrodialysis for an energy conversion system, Electrochem. Commun. 72 (Supplement C) (2016) 157–161.
[5] P.A. Pissoort, in: M.D.C.E.D. L'INDUSTRIE (Ed.), Accumulateur électrique, 1933. France.
[6] W. Kangro, Verfahren zur Speicherung von elektrischer Energie A process for storing electrical energy, in: Deutsches Patentamt, 1954. Germany.
[7] A. Posner, Redox fuel cell, Fuel 34 (3) (1955) 330–338.
[8] M.A. Vertes, et al., Zinc/Air High Energy Density Rechargeable Energy Storage System, Defense Technical Information Center, Ft. Belvoir, 1966.
[9] S. Ashimura, Y. Miyake, Denki Kagaku 39 (1971) 977.
[10] S. Ashimura, Y. Miyake, in: Denki Kagaku 43, 1975, p. 214.
[11] S. Ashimura, Y. Miyake, in: Denki Kagaku 44, 1976, p. 50.
[12] G. Ciprios, W.E. Jr, P.G. Grimes, in: NASA Contract Rep. No. NAS3-135-206, 1977, pp. 1–2.
[13] J. Giner, L. Swette, K. Cahill, NASA Contract NAS3-19760, NASA CR-134705, 1976.
[14] Thaller, L.H. in Ninth Intersoc. Energy Conv. Eng. Conf. 1974. San Francisco, CA.
[15] P.M. O'Donnell, R.F. Gahn, W. Pfeiffer, Twelfth Photovoltaic Specialists Conf, Baton Rouge, Louisiana, 1976.
[16] M. Skyllas-Kazacos, et al., New all-vanadium redox flow cell, J. Electrochem. Soc. 133 (5) (1986) 1057–1058.
[17] I.E.O., U.S. Energy Information Administration, 2017.
[18] S.N. Laboratories, DOE global energy storage database. DOE global energy storage, Database (2016), https://doi.org/10.1109/POWERCON.2016.7754009 [cited 2018 1/15/2018]; Available from: http://www.energystorageexchange.org/.
[19] I. Gyuk, et al., Grid energy storage, U.S. Department of Energy, 2013.
[20] J. Noack, et al., Techno-economic modeling and analysis of redox flow battery systems, Energies 9 (8) (2016).
[21] L. Brandeis, et al., in: Analysis of Electrical Energy Storage Technologies for Future Electric Grids, 2016, pp. 513–518.
[22] Z. González, et al., Outstanding electrochemical performance of a graphene-modified graphite felt for vanadium redox flow battery application, J. Power Sources 338 (2017) 155–162.
[23] L. Zeng, et al., Highly stable pyridinium-functionalized cross-linked anion exchange membranes for all vanadium redox flow batteries, J. Power Sources 331 (Supplement C) (2016) 452–461.
[24] P.K. Leung, et al., Membrane-less hybrid flow battery based on low-cost elements, J. Power Sources 341 (2017) 36–45.
[25] Z. Li, et al., Air-breathing aqueous sulfur flow battery for ultralow-cost long-duration electrical storage, Joule 1 (2) (2017) 306–327.
[26] D. Lloyd, et al., Preparation of a cost-effective, scalable and energy efficient all-copper redox flow battery, J. Power Sources 292 (Supplement C) (2015) 87–94.
[27] T.J. Petek, et al., Slurry electrodes for iron plating in an all-iron flow battery, J. Power Sources 294 (Supplement C) (2015) 620–626.
[28] Y.K. Zeng, et al., A low-cost iron-cadmium redox flow battery for large-scale energy storage, J. Power Sources 330 (Supplement C) (2016) 55–60.
[29] Y.K. Zeng, et al., A comparative study of all-vanadium and iron-chromium redox flow batteries for large-scale energy storage, J. Power Sources 300 (2015) 438–443.
[30] G.L. Soloveichik, Flow batteries: curent status and trends, Chem. Rev. 115 (2015) 11533–11558.
[31] R.M. Darling, et al., Pathways to low-cost electrochemical energy storage: a comparison of aqueous and nonaqueous flow batteries, Energy Environ. Sci. 7 (11) (2014) 3459–3477.
[32] Y. Huang, et al., Nonaqueous redox-flow batteries: features, challenges, and prospects, Curr. Opin. Chem. Eng. 8 (2015) 105–113.
[33] P. Leung, et al., Progress in redox flow batteries, remaining challenges and their applications in energy storage, RSC Adv. 2 (27) (2012) 10125–10156.
[34] W. Wang, et al., Recent Progress in redox flow battery Research and Development, Adv. Funct. Mater. 23 (8) (2013) 970–986.
[35] P. Leung, et al., Cyclohexanedione as the negative electrode reaction for aqueous organic redox flow batteries, Appl. Energy 197 (Supplement C) (2017) 318–326.
[36] S. Gentil, D. Reynard, H.H. Girault, Aqueous organic and redox-mediated redox flow batteries: a review, Curr. Opin. Electrochem. 21 (2020) 7–13.
[37] Q. Zheng, et al., Dramatic performance gains of a novel circular vanadium flow battery, J. Power Sources 277 (2015) 104–109.
[38] S. Ressel, et al., Performance of a vanadium redox flow battery with tubular cell design, J. Power Sources 355 (2017) 199–205.
[39] W.J. van Egmond, et al., The concentration gradient flow battery as electricity storage system: technology potential and energy dissipation, J. Power Sources 325 (Supplement C) (2016) 129–139.
[40] A. Bhattarai, et al., Advanced porous electrodes with flow channels for vanadium redox flow battery, J. Power Sources 341 (2017) 83–90.
[41] E. Zanzola, et al., Redox solid energy boosters for flow batteries: polyaniline as a case study, Electrochim. Acta 235 (Supplement C) (2017) 664–671.
[42] J. Houser, et al., Influence of architecture and material properties on vanadium redox flow battery performance, J. Power Sources 302 (Supplement C) (2016) 369–377.
[43] D. Reed, et al., Stack developments in a kW class all vanadium mixed acid redox flow battery at the Pacific Northwest National Laboratory, J. Electrochem. Soc. 163 (1) (2016) A5211–A5219.
[44] S. Kumar, S. Jayanti, Effect of flow field on the performance of an all-vanadium redox flow battery, J. Power Sources 307 (Supplement C) (2016) 782–787.
[45] S. Liao, et al., Photoelectrochemical regeneration of all vanadium redox species for construction of a solar rechargeable flow cell. Journal of energy, Chemistry 27 (1) (2018) 278–282.
[46] Z. Wei, et al., Geometry-enhanced ultra-long TiO2 nanobelts in an all-vanadium photoelectrochemical cell for efficient storage of solar energy, Nano Energy 26 (2016) 200–207.
[47] Y. Shen, et al., All-vanadium photoelectrochemical storage cells using dye sensitized geometry-enhanced TiO2 nanobelts, Mater. Res. Bull. 96 (Part 4) (2017) 431–436.
[48] D.M. Kabtamu, et al., Water-activated graphite felt as a high-performance electrode for vanadium redox flow batteries, J. Power Sources 341 (2017) 270–279.
[49] J.-Z. Chen, et al., All-vanadium redox flow batteries with graphite felt electrodes treated by atmospheric pressure plasma jets, J. Power Sources 274 (Supplement C) (2015) 894–898.
[50] L. Wei, et al., Copper nanoparticle-deposited graphite felt electrodes for all vanadium redox flow batteries, Appl. Energy 180 (2016) 386–391.
[51] M. Kim, et al., Enhanced VRB electrochemical performance using tungsten as an electrolyte additive, Electrochim. Acta 246 (2017) 190–196.
[52] L. Wei, et al., Highly catalytic and stabilized titanium nitride nanowire array-decorated graphite felt electrodes for all vanadium redox flow batteries, J. Power Sources 341 (2017) 318–326.
[53] L. Wei, et al., A high-performance carbon nanoparticle-decorated graphite felt electrode for vanadium redox flow batteries, Appl. Energy 176 (2016) 74–79.
[54] H. Kabir, I.O. Gyan, I. Francis Cheng, Electrochemical modification of a pyrolytic graphite sheet for improved negative electrode performance in the vanadium redox flow battery, J. Power Sources 342 (Supplement C) (2017) 31–37.
[55] J. Kim, et al., High electrocatalytic performance of N and O atomic co-functionalized carbon electrodes for vanadium redox flow battery, Carbon 111 (Supplement C) (2017) 592–601.
[56] Y. Huang, et al., N, O co-doped carbon felt for high-performance all-vanadium redox flow battery, Int. J. Hydrog. Energy 42 (10) (2017) 7177–7185.
[57] M. Jing, et al., CeO2 embedded electrospun carbon nanofibers as the advanced electrode with high effective surface area for vanadium flow battery, Electrochim. Acta 215 (Supplement C) (2016) 57–65.
[58] H.R. Jiang, et al., Highly active, bi-functional and metal-free B4C-nanoparticle-modified graphite felt electrodes for vanadium redox flow batteries, J. Power Sources 365 (Supplement C) (2017) 34–42.

[59] Z.H. Zhang, et al., A highly active biomass-derived electrode for all vanadium redox flow batteries, Electrochim. Acta 248 (2017) 197–205.
[60] N.C. Hoyt, et al., Plating utilization of carbon felt in a hybrid flow battery, J. Electrochem. Soc. 163 (1) (2016) 5041–5048.
[61] H. Yousofian-Varzaneh, H.R. Zare, M. Namazian, Application of tetrafluoro-p-hydroquinone and 3-fluorocatechol as the catholyte and cd nanoparticles as anolyte electroactive materials to manufacture of hybrid redox flow batteries, J. Electroanal. Chem. 776 (Supplement C) (2016) 193–201.
[62] J. Sun, et al., Investigations on the self-discharge process in vanadium flow battery, J. Power Sources 294 (2015) 562–568.
[63] X.L. Zhou, et al., Performance of a vanadium redox flow battery with a VANADion membrane, Appl. Energy 180 (Supplement C) (2016) 353–359.
[64] L. Zeng, et al., Polyvinylpyrrolidone-based semi-interpenetrating polymer networks as highly selective and chemically stable membranes for all vanadium redox flow batteries, J. Power Sources 327 (Supplement C) (2016) 374–383.
[65] Z. Yuan, et al., Highly stable aromatic poly (ether sulfone) composite ion exchange membrane for vanadium flow battery, J. Membr. Sci. 541 (Supplement C) (2017) 465–473.
[66] T. Luo, et al., Porous poly(benzimidazole) membrane for all vanadium redox flow battery, J. Power Sources 312 (2016) 45–54.
[67] Z. Xia, et al., Preparation of covalently cross-linked sulfonated polybenzimidazole membranes for vanadium redox flow battery applications, J. Membr. Sci. 525 (2017) 229–239.
[68] L. Chen, et al., Low vanadium ion permeabilities of sulfonated poly (phthalazinone ether ketone)s provide high efficiency and stability for vanadium redox flow batteries, J. Power Sources 355 (2017) 23–30.
[69] T.D. Largier, C.J. Cornelius, Random quaternary ammonium diels-Alder poly (phenylene) copolymers for improved vanadium redox flow batteries, J. Power Sources 352 (2017) 149–155.
[70] Y. Ji, Z.Y. Tay, S.F.Y. Li, Highly selective sulfonated poly(ether ether ketone)/titanium oxide composite membranes for vanadium redox flow batteries, J. Membr. Sci. 539 (Supplement C) (2017) 197–205.
[71] C. Wu, et al., Enhanced membrane ion selectivity by incorporating graphene oxide nanosheet for vanadium redox flow battery application, Electrochim. Acta 248 (2017) 454–461.
[72] J. Kim, J.-D. Jeon, S.-Y. Kwak, Sulfonated poly(ether ether ketone) composite membranes containing microporous layered silicate AMH-3 for improved membrane performance in vanadium redox flow batteries, Electrochim. Acta 243 (2017) 220–227.
[73] T. Sadhasivam, et al., Low permeable composite membrane based on sulfonated poly(phenylene oxide) (sPPO) and silica for vanadium redox flow battery, Int. J. Hydrog. Energy 42 (30) (2017) 19035–19043.
[74] M.S. Cha, et al., Crosslinked anion exchange membranes with primary diamine-based crosslinkers for vanadium redox flow battery application, J. Power Sources 363 (Supplement C) (2017) 78–86.
[75] B. Zhang, et al., Quaternized adamantane-containing poly(aryl ether ketone) anion exchange membranes for vanadium redox flow battery applications, J. Power Sources 325 (Supplement C) (2016) 801–807.
[76] S. Yun, J. Parrondo, V. Ramani, Composite anion exchange membranes based on quaternized cardo-poly(etherketone) and quaternized inorganic fillers for vanadium redox flow battery applications, Int. J. Hydrog. Energy 41 (25) (2016) 10766–10775.
[77] B. Zhang, et al., Poly(phenyl sulfone) anion exchange membranes with pyridinium groups for vanadium redox flow battery applications, J. Power Sources 282 (Supplement C) (2015) 328–334.
[78] S. Souentie, et al., Temperature, charging current and state of charge effects on iron-vanadium flow batteries operation, Appl. Energy 206 (Supplement C) (2017) 568–576.
[79] W. Lee, et al., Iron-vanadium redox flow batteries with polybenzimidazole membranes: high coulomb efficiency and low capacity loss, J. Power Sources 439 (2019), 227079.
[80] Y.K. Zeng, et al., A high-performance flow-field structured iron-chromium redox flow battery, J. Power Sources 324 (Supplement C) (2016) 738–744.
[81] Y.K. Zeng, et al., Performance enhancement of iron-chromium redox flow batteries by employing interdigitated flow fields, J. Power Sources 327 (Supplement C) (2016) 258–264.
[82] A. Orita, et al., The impact of pH on side reactions for aqueous redox flow batteries based on nitroxyl radical compounds, J. Power Sources 321 (Supplement C) (2016) 126–134.
[83] Z. Na, et al., A cerium–lead redox flow battery system employing supporting electrolyte of methanesulfonic acid, J. Power Sources 295 (Supplement C) (2015) 28–32.
[84] A.N. Colli, P. Peljo, H.H. Girault, High energy density MnO4-/MnO42- redox couple for alkaline redox flow batteries, Chem. Commun. 52 (97) (2016) 14039–14042.
[85] N. Chen, et al., SiO2-decorated graphite felt electrode by silicic acid etching for iron-chromium redox flow battery, Electrochim. Acta 336 (2020), 135646.
[86] B.H. Robb, J.M. Farrell, M.P. Marshak, Chelated chromium electrolyte enabling high-voltage aqueous flow batteries, Joule 3 (10) (2019) 2503–2512.
[87] M. Rahimi, A. Molaei Dehkordi, E.P.L. Roberts, Magnetic nanofluidic electrolyte for enhancing the performance of polysulfide/iodide redox flow batteries, Electrochim. Acta (2021) 369.
[88] Y. Liu, et al., An aqueous redox flow battery with a tungsten-cobalt heteropolyacid as the electrolyte for both the anode and cathode, Adv. Energy Mater. 7 (8) (2017) 1601224.
[89] Y. Liu, et al., The effect of nafion membrane thickness on performance of all tungsten-cobalt heteropoly acid redox flow battery, J. Power Sources 392 (2018) 260–264.
[90] J. Luo, et al., Unraveling pH dependent cycling stability of ferricyanide/ferrocyanide in redox flow batteries, Nano Energy 42 (Supplement C) (2017) 215–221.
[91] N. Kocyigit, et al., A novel vanadium/cobalt redox couple in aqueous acidic solution for redox flow batteries, Int. J. Energy Res. 44 (1) (2020) 411–424.
[92] M. Etienne, et al., layer-by-layer modification of graphite felt with MWCNT for vanadium redox flow battery, Electrochim. Acta 313 (2019) 131–140.
[93] Q. Wu, et al., An improved thin-film electrode for vanadium redox flow batteries enabled by a dual layered structure, J. Power Sources 410–411 (2019) 152–161.
[94] M. Jing, et al., Anchoring effect of the partially reduced graphene oxide doped electrospun carbon nanofibers on their electrochemical performances in vanadium flow battery, J. Power Sources 425 (2019) 94–102.
[95] T. Wang, et al., Selective ion transport for a vanadium redox flow battery (VRFB) in nano-crack regulated proton exchange membranes, J. Membr. Sci. 583 (2019) 16–22.
[96] C. Youn, et al., Effect of nitrogen functionalization of graphite felt electrode by ultrasonication on the electrochemical performance of vanadium redox flow battery, Mater. Chem. Phys. 237 (2019), 121873.
[97] Y. Xiang, W.A. Daoud, Investigation of an advanced catalytic effect of cobalt oxide modification on graphite felt as the positive electrode of the vanadium redox flow battery, J. Power Sources 416 (2019) 175–183.
[98] W. Duan, et al., Towards an all-vanadium redox flow battery with higher theoretical volumetric capacities by utilizing the VO2+/V3+ couple, J. Energy Chem. 27 (5) (2018) 1381–1385.
[99] J. Si, et al., Microscopic phase-segregated quaternary ammonia polysulfone membrane for vanadium redox flow batteries, J. Power Sources 428 (2019) 88–92.
[100] F. Jiang, et al., Carbon aerogel modified graphite felt as advanced electrodes for vanadium redox flow batteries, J. Power Sources 440 (2019), 227114.
[101] S. Kumar, M. Bhushan, V.K. Shahi, Cross-linked amphoteric membrane: sulphonated poly(ether ether ketone) grafted with 2,4,6-tris(dimethylamino-methyl)phenol using functionalized side chain spacers for vanadium redox flow battery, J. Power Sources 448 (2020), 227358.
[102] K. Geng, et al., A novel polybenzimidazole membrane containing bulky naphthalene group for vanadium flow battery, J. Membr. Sci. 586 (2019) 231–239.
[103] X.H. Yan, et al., A highly selective proton exchange membrane with highly ordered, vertically aligned, and subnanosized 1D channels for redox flow batteries, J. Power Sources 406 (2018) 35–41.
[104] X. Yan, et al., A highly proton-conductive and vanadium-rejected long-side-chain sulfonated polybenzimidazole membrane for redox flow battery, J. Membr. Sci. 596 (2020), 117616.
[105] J. Sun, et al., Formation of electrodes by self-assembling porous carbon fibers into bundles for vanadium redox flow batteries, J. Power Sources 405 (2018) 106–113.
[106] L. Zeng, et al., A promising SPEEK/MCM composite membrane for highly efficient vanadium redox flow battery, Surf. Coat. Technol. 358 (2019) 167–172.
[107] L. Qiao, et al., Advanced porous membranes with slit-like selective layer for flow battery, Nano Energy 54 (2018) 73–81.
[108] Y. Ma, et al., Cyclodextrin templated nanoporous anion exchange membrane for vanadium flow battery application, J. Membr. Sci. 586 (2019) 98–105.
[109] L. Ding, et al., Enhancing proton conductivity of polybenzimidazole membranes by introducing sulfonate for vanadium redox flow batteries applications, J. Membr. Sci. 578 (2019) 126–135.
[110] B. Zhang, et al., High performance membranes based on new 2-adamantane containing poly(aryl ether ketone) for vanadium redox flow battery applications, J. Power Sources 399 (2018) 18–25.
[111] K.I. Jeong, S.A. Song, S.S. Kim, Glucose-based carbon-coating layer on carbon felt electrodes of vanadium redox flow batteries, Compos. Part B 175 (2019), 107072.
[112] L. Sanz, et al., Study and characterization of positive electrolytes for application in the aqueous all-copper redox flow battery, J. Power Sources 278 (Supplement C) (2015) 175–182.
[113] Y.K. Zeng, et al., A novel iron-lead redox flow battery for large-scale energy storage, J. Power Sources 346 (2017) 97–102.
[114] M. Krishna, et al., Measurement of key electrolyte properties for improved performance of the soluble lead flow battery, Int. J. Hydrog. Energy 42 (29) (2017) 18491–18498.
[115] S. Rathod, et al., Effect of binary additives on performance of the undivided soluble-lead-redox-flow battery, Electrochim. Acta 365 (2021), 137361.
[116] S. Selverston, R.F. Savinell, J.S. Wainright, Zinc-iron flow batteries with common electrolyte, J. Electrochem. Soc. 164 (6) (2017) A1069–A1075.
[117] B. Li, et al., Ambipolar zinc-polyiodide electrolyte for a high-energy density aqueous redox flow battery, Nat. Commun. 6 (2015) 6303.
[118] M. Mousavi, et al., Decoupled low-cost ammonium-based electrolyte design for highly stable zinc–iodine redox flow batteries, Energy Storage Materials 32 (2020) 465–476.
[119] H.S. Yang, et al., Critical rate of electrolyte circulation for preventing zinc dendrite formation in a zinc–bromine redox flow battery, J. Power Sources 325 (Supplement C) (2016) 446–452.
[120] M.C. Wu, et al., High-performance zinc bromine flow battery via improved design of electrolyte and electrode, J. Power Sources 355 (2017) 62–68.

[121] J.H. Yang, et al., Effect of a surface active agent on performance of zinc/bromine redox flow batteries: improvement in current efficiency and system stability, J. Power Sources 275 (Supplement C) (2015) 294–297.
[122] G. Tomazic, M. Skyllas-Kazacos, Chapter 17 - Redox flow batteries, in: P. T. Moseley, J. Garche (Eds.), Electrochemical Energy Storage for Renewable Sources and Grid Balancing, Elsevier, Amsterdam, 2015, pp. 309–336.
[123] R. Chen, R. Hempelmann, Ionic liquid-mediated aqueous redox flow batteries for high voltage applications, Electrochem. Commun. 70 (Supplement C) (2016) 56–59.
[124] L.F. Arenas, C.P.d. León, F.C. Walsh, Mass transport and active area of porous Pt/Ti electrodes for the Zn-Ce redox flow battery determined from limiting current measurements, Electrochimica Acta 221 (Supplement C) (2016) 154–166.
[125] K. Amini, M.D. Pritzker, In situ polarization study of zinc–cerium redox flow batteries, J. Power Sources 471 (2020), 228463.
[126] M.C. Karaeyvaz, B. Duman, B. Fıçıcılar, An alternative HCMS carbon catalyst in bromine reduction reaction for hydrogen-bromine flow batteries, Int. J. Hydrog. Energy 46 (57) (2020) 29512–29522.
[127] S. Suresh, M. Ulaganathan, R. Pitchai, Realizing highly efficient energy retention of Zn–Br2 redox flow battery using rGO supported 3D carbon network as a superior electrode, J. Power Sources 438 (2019), 226998.
[128] M.C. Wu, et al., N-doped graphene nanoplatelets as a highly active catalyst for Br 2/Br− redox reactions in zinc-bromine flow batteries, Electrochim. Acta 318 (2019) 69–75.
[129] M.C. Wu, et al., Carbonized tubular polypyrrole with a high activity for the br 2/Br− redox reaction in zinc-bromine flow batteries, Electrochim. Acta 284 (2018) 569–576.
[130] M. Kim, D. Yun, J. Jeon, Effect of a bromine complex agent on electrochemical performances of zinc electrodeposition and electrodissolution in zinc-bromide flow battery, J. Power Sources 438 (2019), 227020.
[131] S. Bae, J. Lee, D.S. Kim, The effect of Cr3+-functionalized additive in zinc-bromine flow battery, J. Power Sources 413 (2019) 167–173.
[132] Y. Cheng, et al., A long-life hybrid zinc flow battery achieved by dual redox couples at cathode, Nano Energy 63 (2019), 103822.
[133] Y. Cheng, et al., Efficient unitary oxygen electrode for air-based flow batteries, Nano Energy 47 (2018) 361–367.
[134] D.P. Trudgeon, et al., Screening of effective electrolyte additives for zinc-based redox flow battery systems, J. Power Sources 412 (2019) 44–54.
[135] Y. Zhang, et al., Enhanced reaction kinetics of an aqueous Zn–Fe hybrid flow battery by optimizing the supporting electrolytes, J. Energy Storage 25 (2019), 100883.
[136] S. Chang, et al., A low-cost SPEEK-K type membrane for neutral aqueous zinc-iron redox flow battery, Surf. Coat. Technol. 358 (2019) 190–194.
[137] S.T. Senthilkumar, et al., Energy efficient Na-aqueous-catholyte redox flow battery, Energy Storage Mater. 12 (2017) 324–330.
[138] T. Liu, et al., A Total organic aqueous redox flow battery employing a low cost and sustainable methyl viologen anolyte and 4-HO-TEMPO catholyte, Adv. Energy Mater. 6 (3) (2016) 1501449.
[139] W.J. van Egmond, et al., Energy efficiency of a concentration gradient flow battery at elevated temperatures, J. Power Sources 340 (Supplement C) (2017) 71–79.
[140] R.S. Kingsbury, K. Chu, O. Coronell, Energy storage by reversible electrodialysis: the concentration battery, J. Membr. Sci. 495 (Supplement C) (2015) 502–516.
[141] A. Sáez, V. Montiel, A. Aldaz, An acid-base electrochemical flow battery as energy storage system, Int. J. Hydrog. Energy 41 (40) (2016) 17801–17806.
[142] Q. Wang, et al., Redox targeting of insulating electrode materials: a new approach to high-energy-density batteries, Angew. Chem. 118 (48) (2006) 8377–8380.
[143] C.M. Wong, C.S. Sevov, All-organic storage solids and redox shuttles for redox-targeting flow batteries, ACS Energy Lett. 6 (4) (2021) 1271–1279.
[144] Y. Zhen, et al., A high-performance all-iron non-aqueous redox flow battery, J. Power Sources 445 (2020), 227331.
[145] H. Zhang, et al., Investigations on physicochemical properties and electrochemical performance of graphite felt and carbon felt for iron-chromium redox flow battery, Int. J. Energy Res. 44 (5) (2020) 3839–3853.
[146] B. Yu, et al., Study of simultaneously electrodepositing α/β-PbO2 coating materials in methanesulfonic acid and its application in novel flow battery, Renew. Energy 159 (2020) 885–892.
[147] B. Kim, J.Y. Seo, C.-H. Chung, A hybrid system of capacitive deionization and redox flow battery for continuous desalination and energy storage, J. Power Sources 448 (2020), 227384.
[148] J. Gouveia, et al., Life cycle assessment of a vanadium flow battery, Energy Rep. 6 (2020) 95–101.
[149] Y. Xue, et al., Flow battery control strategy implementation and cost benefit analysis for microgrid under updated time-of-use periods, in: 2020 IEEE Power & Energy Society Innovative Smart Grid Technologies Conference (ISGT), IEEE, 2020.
[150] C. Choi, et al., A review of vanadium electrolytes for vanadium redox flow batteries, Renew. Sust. Energ. Rev. 69 (2017) 263–274.
[151] S.E. Waters, B.H. Robb, M.P. Marshak, Effect of chelation on iron-chromium redox flow batteries, ACS Energy Lett. 5 (6) (2020) 1758–1762.
[152] W. Huang, Q. Zou, Y.C. Lu, Ion-selective membrane-free dual sulfur-iodine catholyte for low-cost and high-power flow battery applications, Batteries Supercaps 2 (11) (2019) 941–947.
[153] P. Leung, et al., Evaluation of electrode materials for all-copper hybrid flow batteries, J. Power Sources 310 (2016) 1–11.
[154] A. Khor, et al., Review of zinc-based hybrid flow batteries: from fundamentals to applications, Mater. Today Energy 8 (2018) 80–108.
[155] C.B. Jeena, et al., A dendrite free Zn-Fe hybrid redox flow battery for renewable energy storage, Energy Storage 4 (1) (2022), e275.
[156] P.K. Leung, C. Ponce de León, F.C. Walsh, An undivided zinc–cerium redox flow battery operating at room temperature (295 K), Electrochem. Commun. 13 (8) (2011) 770–773.